

Bayesian Reassessment of Seismic Moment Tensors and Their Uncertainties in the Adriatic Sea Region

Jinyin Hu * 📵¹, Hrvoje Tkalčić 📵¹, Thanh-Son Phạm 📵¹, Marijan Herak 📵², Iva Dasović 📵², Marija Mustać Brčić 📵²

¹Research School of Earth Sciences, The Australian National University, Canberra, ACT, Australia, ²Department of Geophysics, Faculty of Science, University of Zagreb, Zagreb, Croatia

Author contributions: Conceptualization: Jinyin Hu, Hrvoje Tkalčić. Data Curation: Jinyin Hu, Iva Dasović. Formal Analysis: All authors. Funding Acquisition: Hrvoje Tkalčić. Investigation: All authors. Methodology: Jinyin Hu, Hrvoje Tkalčić, Thanh-Son Phạm. Project Administration: Hrvoje Tkalčić. Resources: Hrvoje Tkalčić. Software: Jinyin Hu, Thanh-Son Phạm. Supervision: Hrvoje Tkalčić, Thanh-Son Phạm. Validation: All authors. Visualization: All authors. Writing - original draft: Jinyin Hu, Hrvoje Tkalčić, Marija Mustać Brčić. Writing - review & editing: All authors.

Abstract The determination of seismic moment tensor (MT) parameters is subject to uncertainties from data noise and structural error due to the imperfect Earth model, which is rarely considered in regional earth-quake catalogs. In this study, we apply a hierarchical Bayesian MT inversion with uncertainty quantification to seven moderate-earthquakes (M_w 4.5–5.5) in the Adriatic Sea region. The event collection includes three in mainland Croatia: the 2020 M_w 5.4 Zagreb earthquake and its M_w 4.9 aftershock, and the M_w 5.0 foreshock of the 2020 Petrinja earthquake, two events in the offshore Adriatic Sea: the 2021 M_w 5.2 central Adriatic earthquake, the 2024 M_w 4.6 southern Adriatic earthquake, and two in Italy: the 2022 M_w 5.5 Costa Marchigiana-Pesarese earthquake, and the 2023 M_w 4.9 earthquake in Marradi (Tuscany). The inversion output features the source depth and the posterior distributions of the MT parameters, enabling the uncertainty quantification. Comparing our results with regional routine catalogs highlights the improvement in source determination, particularly in confidence of non-double-couple components when incorporating the data and structural uncertainties. The refined source mechanisms could be useful for understanding the complex geological settings, assessing the hazard potential, and further improving the regional earthquake catalogs in the Adriatic Sea region.

Production Editor: Yen Joe Tan Handling Editor: Wenbin Xu Copy & Layout Editor: Sarah Jaye Oliva

> Signed reviewer(s): Jan Šíleny Angela Sarao

Received:
May 12, 2025
Accepted:
October 12, 2025
Published:
November 26, 2025

1 Introduction

The determination of earthquake source mechanisms relies on seismic inversion, a numerical procedure that infers the source parameters using recorded seismic waveforms and available Earth models. For small to moderate earthquakes, the earthquake sources are commonly represented by the point-source moment tensor (MT), a 3 × 3 symmetric matrix of six independent force couples. A full MT can be decomposed into double couple (DC) and non-double couple (non-DC) components, the latter comprising isotropic (ISO) and compensated linear vector dipole (CLVD) components according to Knopoff and Randall (1970) and others (e.g., Sipkin, 1986; Vavryčuk, 2014). The DC component represents shear slip on planar faults, which is typical of most tectonic earthquakes, while the non-DC components have more complicated causes and implications. The non-DC may originate from intrinsic source processes, the combined effect of DC processes, or they may be an artifact of the inversion (e.g., Rösler and Stein, 2022). In well-documented non-DC events, the ISO component reflects explosions or implosions causing volume changes (e.g., Alvizuri and Tape, 2018) and the CLVD component is often linked to magma movement in volcanic environments (e.g., Dreger et al., 2000). A comprehensive overview of MT decomposition and non-DC sources can be found in Julian et al. (1998).

The determination of the relative significance of the MT compositions is important in characterizing the physical nature of seismic sources. Rapid seismic source inversion of MT parameters has been established as a routine procedure in seismology, and the attention has shifted towards uncertainty quantification of the solutions, which is featured in this work.

The two primary sources of uncertainty in seismic source inversion are data noise, which is inherited from the data acquisition and processing stages, and the error due to imperfect theory, dominated by inaccuracies in Green's functions caused by the simplified description of the Earth's interior, also known as model error or structural error. A rigorous uncertainty treatment for data noise and structural error is crucial for enhancing the reliability of MT parameter solutions. Many efforts have been made to consider data noise (e.g., Duputel et al., 2012; Mustać et al., 2018, 2020; Mustać and Tkalčić, 2016, 2017; Saoulis et al., 2025) and structural error (e.g., Hallo and Gallovič, 2016) separately. The most recent advancements are in jointly treating these two classes of uncertainty in MT inversion (e.g., Pham et al., 2024; Pham and Tkalčić, 2021; Vasyura-Bathke

^{*}Corresponding author: Jinyin.hu@anu.edu.au

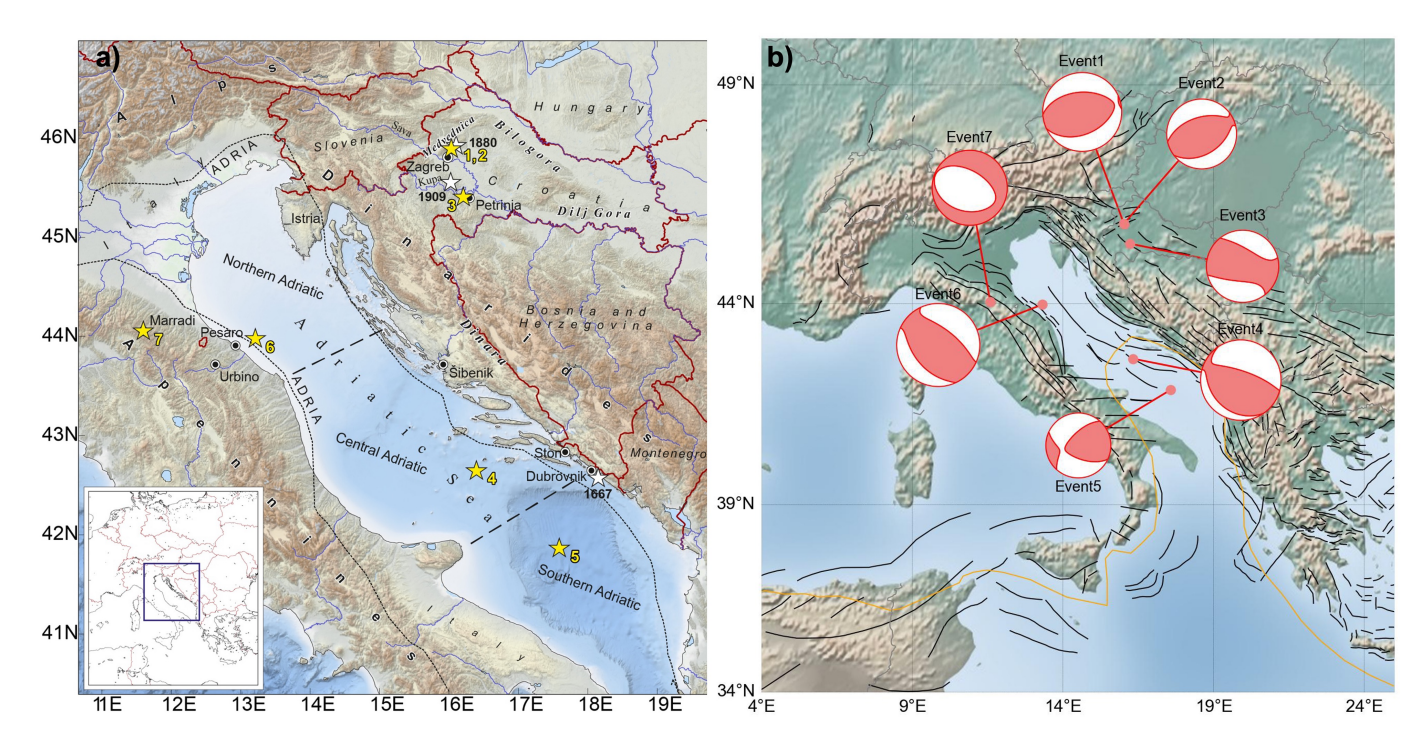


Figure 1 (a) Overview map of the studied region with its position in Europe marked by the blue rectangle in the inset. Approximate Adria margins are indicated by black dotted lines. The most important historical earthquakes mentioned in text are shown by white stars, together with the year of occurrence. The seven studied earthquakes are shown by yellow stars, with numbers corresponding to the event numbers in Table 1. (b) MT solutions from the MT inversion in this study for seven selected earthquakes. For each event, the beachball represents the recovered deviatoric MT solution. The size of the beachball is scaled proportionally to the corresponding moment magnitude. Black lines on the map indicate the known faults in this region, as documented in the European Database of Seismogenic Faults (Basili et al., 2013). The yellow line is the tectonic plate boundary.

et al., 2021). However, uncertainty quantification is yet to be fully incorporated in regional earthquake catalogs.

We recently developed Bayesian inversion methods to estimate MT parameters, incorporating uncertainties stemming from heterogeneities in the Earth structure models and station-specific noise in seismic waveforms (Hu et al., 2023, 2024). Our approach utilizes a lightweight scheme to treat the structural error by applying station-specific time shifts as free parameters to re-align predicted waveforms with the observations, so it has the potential for routine analysis of many events. In this proof-of-concept work, we apply this method to reassess the MT parameters of moderate-size earthquakes in the Adriatic Sea region, motivated by its complex tectonic setting (discussed in the Study Area section) and the diversity of the observed focal mechanisms.

In this study, we selected seven earthquakes with reported moment magnitudes (M_w) between 4.5 and 5.5 that occurred over the past five years in the Adriatic Sea and the surrounding Croatia and Italy. They are labeled as Events 1–7 in Fig. 1 and listed in Table 1. They include two earthquakes in mainland Croatia: the 2020 M_w 5.4 Zagreb earthquake and its largest M_w 4.9 aftershock, the largest M_w 5.0 foreshock of the 2020 M_w 6.4 Petrinja earthquake, and two in the offshore Adriatic Sea: the 2021 M_w 5.2 central Adriatic earthquake, and the 2024 M_w 4.6 southern Adriatic earthquake. The other two events are in Italy: the 2022 M_w 5.5 earthquake in Costa Marchigiana Pesarese (Pesaro and Urbino) and the 2023

 M_w 4.9 earthquake in Marradi (Tuscany). By comparing with the solutions from regional catalogs from agencies, such as the Istituto Nazionale di Geofisica e Vulcanologia (INGV, Italy) catalog (Pondrelli, 2002, henceforth referred to as the INGV catalog) last accessed on 10 October 2024 (now possibly outdated), the study's results highlight the improved confidence in the determined solutions for regional applications. The reliable source mechanisms can be helpful in further guiding the interpretation of the complex geological settings around the Adriatic Sea.

2 Study area

The Adriatic Sea region is one of the most debated and geologically complex tectonic settings along the broader margin between the Eurasian and African plates. The semi-enclosed Adriatic Sea basin sits in the middle of this region, surrounded by the Apennines in the southwest and the Dinarides in the northeast. Its complex structural settings are shaped by tectonic activity, sedimentation, and geomorphology (Kastelic et al., 2013; Le Breton et al., 2017; for a review, see Piccardi et al., 2011). The region is formed by the ongoing convergence of the Eurasian and African plates, which drives the counterclockwise rotation and northward movement of the Adriatic microplate (Adria, Fig. 1a). This tectonic interaction leads to the collision and complex deformation between Adria and the Dinarides (and Alps), resulting in seismicity, along the

Event	Origin time (UTC)	Lati- tude (°)	Longi- tude (°)	Depth (km)	Magni- tude	Solution in this study					
						Depth (km)	M_{xx} (10 ¹⁵ N·m	M_{yy} n) (10 15 N·m	M_{xy} n) (10 15 N·m	M_{xz}) (10 ¹⁵ N·m	M_{yz} n) (10 ¹⁵ N·m)
Event 1	2020-03-22 T05:24:03.000Z	45.879	16.028	10.1	M_{w} 5.4	5	-16.007 ±0.161	-0.536 ±0.072	4.215 ±0.044	-2.242 ±0.223	-3.053 ±0.114
Event 2	2020-03-22 T06:01:20.000Z	45.880	16.024	9.4	M_L 4.9	3	-8.738 ±0.085	-1.547 ±0.046	4.376 ±0.048	-2.127 ±0.281	-0.815 ±0.191
Event 3	2020-12-28 T05:28:07.000Z	45.4191	16.2218	9.4	M_L 5.1	8	-17.704 ±0.203	5.523 ±0.133	-8.890 ±0.097	2.759 ±0.168	-4.086 ±0.139
Event 4	2021-03-27 T13:47:51.000Z	42.67	16.33	5	M_w 5.2 (INGV)	4	-52.141 ±0.705	-20.467 ±1.119	-45.070 ±0.435	-91.563 ±2.150	-21.105 ±3.381
Event 5	2024-02-23 T09:23:19.000Z	41.91	17.58	10	M_L 4.7 (INGV)	9	-3.211 ±0.040	1.660 ±0.047	1.048 ±0.030	0.152 ±0.036	1.775 ±0.049
Event 6	2022-11-09 T06:07:25.000Z	43.98	13.32	6	M_w 5.6 (INGV)	6	-98.268 ±1.871	-96.113 ±2.336	-128.675 ±1.336	-71.868 ±4.073	-26.179 ±5.734
Event 7	2023-09-18 T03:10:14.000Z	44.05	11.59	6	M_L 4.9 (INGV)	3	28.776 ±0.211	4.670 ±0.222	10.370 ±0.133	7.212 ±1.000	10.877 ±0.884

Table 1 The seven earthquakes in the Adriatic Sea and its surroundings in Croatia and Italy were analyzed in this study. The origin time is from the INGV catalog (Pondrelli, 2002, last accessed on 10 Oct 2024). The information in columns 2–6 for events 1 and 2, are from Herak et al. (2021b), event 3 is from Herak and Herak (2023), and other events are from INGV (Pondrelli, 2002, last accessed on 10 Oct 2024). Our solutions are presented in columns 7–12, including the source depth from the parameter search, and five MT parameters, each accompanied by uncertainty in the format of mean ± one standard deviation.

northeastern margin of Adria in the Dinarides (Croatia, Slovenia, and Montenegro, e.g., Herak and Herak, 2024; Herak et al., 2005, 1996), and in Italy, particularly along the Apennines and the southwestern Adriatic coast (e.g., Chiarabba et al., 2005; Rovida et al., 2020, 2022). Additionally, intraplate seismicity is observed within both the Eurasian and Adria plates (Fig. 1a).

Seismicity in the Adriatic Sea itself features a distinct pattern that divides the region into three sectors: the northern, central, and southern Adriatic (Fig. 1a). According to Orecchio et al. (2023), the main seismic activity over the past 24 years—up to 2021—occurred in the central Adriatic, where 14 earthquakes with magnitudes M_w 4.0–5.5 were recorded. In the northern sector, seismic events are primarily clustered along the western edge of the Adriatic Sea, particularly near the Italian coastline. In contrast, the southern Adriatic basin typically experiences fewer and weaker earthquakes. Therefore, the cause of the M_L 4.7 earthquake at 09:23 UTC on 23 February 2024 (No. 5 in Fig. 1a) in this region remains uncertain.

In addition, the Croatian coastline is also tectonically complex, comprising two distinct seismicity domains. The northwestern one stretches from NW of Šibenik to the Istria peninsula, while the southeastern (SE) domain spans from Dinara-Kamešnica Mt. to the southern Adriatic Sea (Ivančić et al., 2018). The SE domain includes the greater Dubrovnik epicentral area, which is considered the region with the highest seismic hazard in Croatia. The largest historic earthquake there since records began was the Great Dubrovnik earthquake of 1667 (e.g., Albini, 2015). It was one of the most devastating earthquakes in the broader region, which—along with the large fire that broke out after the earthquake—destroyed most of the city. Two other well-known events happened near the small medieval town of Ston: the

Ston earthquake of 1850 (Herak et al., 2023) and the recent Ston-Slano earthquake of 1996 with M_w 6.0 (Govorčin et al., 2020; Herak and Herak, 2024).

Attention then shifts to the Croatian mainland, where one of the country's most notable recent earthquakes was the 22 March 2020 M_w 5.4 Zagreb earthquake. The mainshock and its aftershock sequence occurred in Croatia's capital, Zagreb, in north-west Croatia. This region lies between the major regional tectonic units of the Alps to the north, the NW Dinarides to the southwest, and the Tisia mega-unit to the east. As a result of complex geological processes, several inselbergs have formed between these units (van Hinsbergen et al., 2020; Schmid et al., 2020). The largest of these is the Medvednica Mountain, with the city of Zagreb located in its southern foothills. It is striking NE–SW, almost orthogonal to the NW–SE trend of the Dinarides (Tomljenović et al., 2008).

The seismicity of NW Croatia is characterized as moderate, with rare occurrences of strong earthquakes (e.g., Ivančić et al., 2018). Over the last few centuries, the entire continental part of Croatia has been struck by a number of notable events, such as the M_L 5.6 1938 Bilogora, and the M_L 5.7 1964 Dilj Gora events. Ivančić et al. (2018) suggested that the whole region was in the stress accumulation phase. Locally, the largest known earthquakes in the Medvednica–Zagreb area before the 2020 earthquake occurred in 1775, 1880, 1906, and 1990 (Herak et al., 2009). Another significant earthquake in the nearby region was the 1909 Kupa Valley earthquake, which led Mohorovičić to discover the Moho discontinuity.

The 1880 event was the largest among these continental events and remains known as the Great Zagreb earthquake. Soon after the earthquake, the Earthquake Committee was formed to document its effects (Torbar, 1882;

Hantken von Prudnik, 1882) (see also Herak and Herak, 2006). The Great Zagreb earthquake resulted in three deaths and damaged nearly all of the 3670 buildings that existed in Zagreb at the time. The maximum intensity is VIII on the EMS-98 scale, and the magnitude estimated from macroseismic data is M_m 6.1. Subsequent earthquake in 1906 was weaker, with magnitude M_L 5.3 calculated from both the macroseismic and the instrumental data (Herak et al., 2021a).

North-western Croatia is one of the three regions in the country with the highest seismic hazard. Furthermore, Zagreb and its surroundings are densely populated with numerous cultural, academic, and political institutions, industrial and commercial facilities, and transport infrastructure. The 2020 earthquake was a harsh reminder of the imposing seismic risk. It caused one casualty, 26 people were severely injured, and there was extensive damage in the historical center of Zagreb. More than 25,500 buildings were inspected by civil engineers, out of which about 35% required short-term repair measures, 20% were temporarily unusable, and 5% were unusable (Atalić et al., 2021; Šavor Novak et al., 2020). The damaged buildings included hospitals, the Croatian parliament, and schools, kindergartens, university buildings, museums, theatres, and sacral buildings. Therefore, understanding the nature of this earthquake can help reduce the damage caused by future earthquakes in the area.

On the opposite side of the Adriatic Sea, the Apennine Peninsula is a highly seismically active region. In just the past four decades, it has been struck by six earthquakes with moment magnitudes $M_w \ge 6.0$, along with several others in the range of $5.5 \le M_w \le 6.0$ —all occurring within seismic sequences that lasted several months to years (Rovida et al., 2020). The seismicity in the region is primarily controlled by Italy's current tectonic setting, which is shaped by multiple factorsincluding the convergence between the Eurasian and African plates, the curvature of the collisional zone at their margins (e.g., D'Agostino et al., 2008), and the broader geodynamic evolution of the Mediterranean region following the closure of the Mesozoic Alpine Tethys (e.g., Handy et al., 2010), etc. Further details are discussed in Latorre et al. (2023) and Palano (2015).

3 Method

Here, we utilize the latest Bayesian MT inversion method, which accounts for uncertainties in data noise and Earth structure model (Hu et al., 2023), to determine the MT parameters for seven representative earthquakes.

The method uses station-specific time shifts between the observed and predicted waveforms as free parameters in the inversion as proxies to account for azimuthal heterogeneities in the region. Hallo and Gallovič (2016) demonstrated that time shifts present a major factor in model uncertainty and reflect the main features of structural heterogeneities in the frequency band typically deployed in the regional MT inversion schemes. They are incorporated in the inversion by shifting the Green's functions in time to improve the match with ob-

served waveforms. The method also accounts for data noise through a diagonal noise covariance matrix by assuming uncorrelated data noise. As noise varies between stations, depending on their proximity to the sea or sources of urban seismic noise, station-specific amplitudes of the data noise covariance matrices are also unknowns to be recovered in the inversion.

The likelihood function of Bayesian inversion includes all information from the data and Earth structure and is proportional to the posterior probability of model parameters. It is defined as

$$p(\mathbf{d}|\mathbf{m}, \mathbf{k}, \mathbf{t}) = \prod_{i=1}^{M} \frac{1}{\sqrt{(2\pi)^{N} |\mathbf{C}_{i}(k_{i})|}} \times \exp \left[-\frac{1}{2} \left(g_{i}(\mathbf{m}, t_{i}) - d_{i} \right)^{T} C_{i}^{-1} \left(g_{i}(\mathbf{m}, t_{i}) - d_{i} \right) \right]$$
(1)

where $\mathbf{m} = [M_{xx}, M_{yy}, M_{xy}, M_{xz}, M_{yz}])$ is a vector of MT parameters with five parameters by restraining deviatoric MTs only, $\mathbf{k}\{k_i\}$ is a vector of station-specific noise parameters included in the covariance matrix \mathbf{C}_i for component i, $\mathbf{t}\{t_i\}$ is the vector of time shifts, also free parameters represented as observed time minus predicted time, g_i (\mathbf{m},t_i) is the shifted predictions and d_i the observed seismogram for component i, M is the number of seismogram components (3 times the number of stations), and N is the number of data points in each seismogram. For the data noise treatment, we use the root mean square of data σ_i as the reference noise strength (e.g., Mustać and Tkalčić, 2016), and construct the data covariance matrix \mathbf{C}_i as

$$\mathbf{C}_{i}\left(k_{i}\right)=\left(k_{i}\sigma_{i}\right)^{2}\mathbf{I}.\tag{2}$$

The posterior probability is numerically estimated by the Markov chain Monte Carlo (McMC) method. The McMC chain generally consists of two stages: the warmup stage, when Bayesian samplers explore the unlikely region of the parameter space with lower posterior probabilities, and the convergence stage, when the samplers examine the highly likely solutions in great details. We conservatively discard the first half of the chain, considered as the warm-up stage, and retain the second half iterations (the convergence stage) as the solution ensemble representative of the posterior distribution. To visualize solution uncertainty, the ensemble is presented in this study as overlapping beach balls and posterior distributions of the parameters. The mean solution of the posterior distribution is then used to analyze the event's characteristics and the comparison with other earthquake catalogs.

4 Data preparation

Using the same inversion scheme, we prepare the waveform data of the seven selected earthquakes (Table 1) from local/regional seismic stations. We mainly use the local network in Croatia for the earthquakes that occur onshore in Croatia, with some supplementary stations in surrounding countries. We downloaded the seismograms from the European Integrated Data Archive

Event	Magnitude (Mw)	DC (%)	CLVD (%)	Nodal plane 1 (°)	Nodal plane 2 (°)
1	5.260 ± 0.003	97.76 ± 0.98	2.24 ± 0.98	$S = 64.2 \pm 0.4$, $D = 43.8 \pm 0.4$, $R = 72.9 \pm 0.5$	$S = 267.3 \pm 0.4$, $D = 48.6 \pm 0.4$, $R = 105.8 \pm 0.5$
2	4.660 ± 0.003	95.29 ± 1.55	4.71 ± 1.55	$S = 55.6 \pm 1.0$, $D = 41.5 \pm 0.7$, $R = 76.2 \pm 1.6$	$S = 253.8 \pm 1.1,$ $D = 50.0 \pm 0.8,$ $R = 101.9 \pm 1.3$
3	4.810 ± 0.003	49.10 ± 1.43	50.90 ± 1.43	$S = 79.7 \pm 0.5,$ $D = 56.3 \pm 0.4,$ $R = 47.3 \pm 0.9$	$S = 318.6 \pm 0.6$, $D = 52.3 \pm 0.5$, $R = 135.5 \pm 0.9$
4	5.360 ± 0.004	94.72 ± 2.45	5.28 ± 2.45	$S = 288.0 \pm 1.5,$ $D = 70.8 \pm 0.4,$ $R = 76.6 \pm 1.1$	$S = 143.9 \pm 1.1,$ $D = 23.2 \pm 0.6,$ $R = 123.6 \pm 2.3$
5	4.330 ± 0.003	96.78 ± 2.22	3.22 ± 2.22	$S = 114.8 \pm 0.6$, $D = 59.3 \pm 0.7$, $R = 149.0 \pm 0.8$	$S = 221.9 \pm 0.4$, $D = 63.7 \pm 0.6$, $R = 34.7 \pm 0.9$
6	5.540 ± 0.004	78.05 ± 2.58	21.95 ± 2.58	$S = 305.2 \pm 1.5,$ $D = 54.9 \pm 0.5,$ $R = 78.1 \pm 1.9$	S = 145.3 ± 1.6, D = 36.8 ± 0.7, R = 106.3 ± 2.5
7	5.000 ± 0.002	87.34 ± 2.03	12.66 ± 2.03	$S = 302.0 \pm 1.4,$ $D = 55.0 \pm 0.5,$ $R = -76.6 \pm 1.9$	$S = 99.4 \pm 1.5$, $D = 37.2 \pm 0.8$, $R = -108.4 \pm 2.3$

Table 2 Results of seven events listed in Table 1, including the percentage of DC and CLVD components, and two nodal planes defined by [strike (S), dip (D), rake (R)]. Uncertainties are reported as mean ± one standard deviation for each parameter.

(https://orfeus-eu.org/data/eida/) hosted by the Observatories and Research Facilities for European Seismology (ORFEUS). The three-component waveform data are then corrected for the instrumental response to obtain displacements and filtered between 20 s and 50 s using a fourth-order one-pass Butterworth filter. Finally, the data is cut into a window centered on the Rayleigh waves based on the origin time in Table 1, specifically, a 120 s window for earthquakes in the Croatian mainland and a 200 s window for earthquakes in the Adriatic Sea and Italy.

We design a criterion modified from Ekström (2006) to select stations for the inversion by adding the weight of epicenter distance. The criterion is based on the combined rank of the station score and the azimuth coverage. The station score is given as

$$score = \overline{SNR} + \overline{D} \tag{3}$$

where \overline{SNR} is the normalized signal-to-noise ratio (SNR) measured by data root-mean-square of the 200 s after and before the P-wave arrival time (Halauwet et al., 2024; Scognamiglio et al., 2009) and \overline{D} is the normalized score for epicenter distance (Scognamiglio et al., 2009) determined considering the earthquake magnitude. Then, the stations are ranked based on the station score, and the first station is selected with the highest rank. The second station is chosen from the rest of the stations, which gives the highest combined rank of station score and the azimuth coverage measured by the effective number of stations, referred to as ENS hereafter,

as defined by Eq. 10 in Ekström (2006). The later stations are chosen one by one following Ekström (2006). The details can be found in the Supplementary Material.

We manually chose 10–12 stations with a high SNR and providing good azimuth coverage for the earth-quakes in the Croatian continental part with the aim to utilize as many stations as possible from Croatia's national network, comprising 30 permanent stations. We use an empirically tested and carefully designed scheme for other earthquakes analyzed in this paper to select eight out of the hundreds of pre-processed stations instead.

The predicted waveforms are processed in the same way as the observed waveforms. They are calculated by following the method developed by Jost and Herrmann (1989), and Minson and Dreger (2008). We compute the Green's functions (GFs) using the frequency-wave number (i.e., f-k) method implementation in Computer Programs in Seismology (Herrmann, 2013) for the source location in Table 1. For earthquakes in the Croatian mainland, we utilize a composite structural model to mitigate the 3-D heterogeneity in the region. The Croatian mainland's geological structure is complex with a significant crustal thickness variation (e.g., Stipčević et al., 2020), necessitating the use of a composite structural model (e.g., Tkalcic et al., 2009) to compute Green's functions. As shown in Fig. S1, four 1-D models are used depending on the station location. For earthquakes in Italy and the Adriatic Sea, we use a 1-D velocity model (a.k.a. CIA; Herrmann et al., 2011), which is

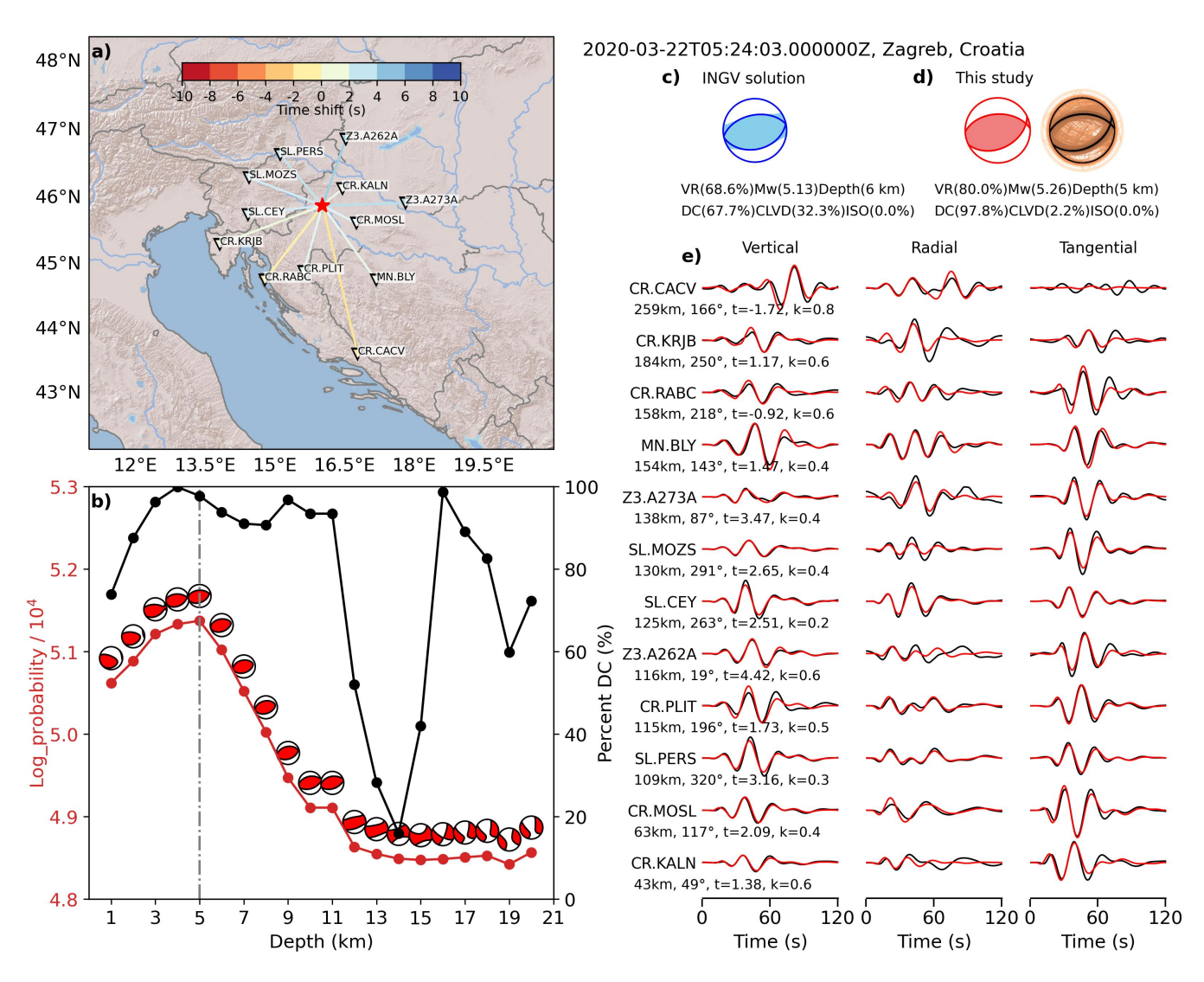


Figure 2 Inversion results for the 2020 Zagreb main shock (Event 1). (a) Map of the study region showing the earthquake location (red star) and the 12 stations (triangles). The colors shown in the color bar denote the recovered station-specific time shifts between observed and predicted waveforms. (b) A parameter search for the source depth from 1 to 20 km in 1 km increment. The red curve (left y-axis) represents the posterior probability of the mean MT (red beachball) in the convergence stage varying with depths, while the black curve (right y-axis) shows the percentage of DC component of the mean MT. The vertical dashed line marks the optimal depth corresponding to the maximum posterior probability. (c) MT solution (beachball) from INGV. (d) MT solutions at the optimal depth in this study, including the mean MT (left) and all MTs during the inversion (right), where yellow represents the warm-up stage, and black represents the convergence stage. (e) Waveform fit between observed (black) and predicted (red) waveforms from the mean MT in (d). The numbers below waveforms are epicenter distance, azimuth, recovered stations-specific time shift, and noise parameters. The listed waveform fit level (VRs) in (c) and (d) are computed by using the GFs from the same composite Earth model, at the same 12 stations, and filtered in the same frequency band, but with each solution's respective source depth.

also used in the INGV catalog to determine the deviatoric MT parameters.

5 Results

The information on the seven earthquakes, along with the source depth from the parameter search in this study and MT solutions with their associated uncertainties, is presented in Table 1. The decomposition of MT solutions, corresponding nodal planes and their associated uncertainties can be found in Table 2. The mean deviatoric MT solution for each earthquake is plotted as a beachball in Fig. 1(b).

As summarized in Figs. 2 and 4–9, panels (a) show the map of earthquake and stations, (b) show the parameter search for source depth, and panels (c) and (d) compare the MT solution from the INGV catalog with the mean MT solution from our inversion. The evolution of MTs during the whole inversion is also visualized by the color-coded beachballs on the right in panel (d), where yellow colors indicate the warm-up stage with lower probabilities, and dark colors indicate the convergence stage with higher probabilities. Panels (e) plot the waveform fit between the observations and predictions generated by the mean MT solution. The recovered station-specific noise parameters k_i and station-

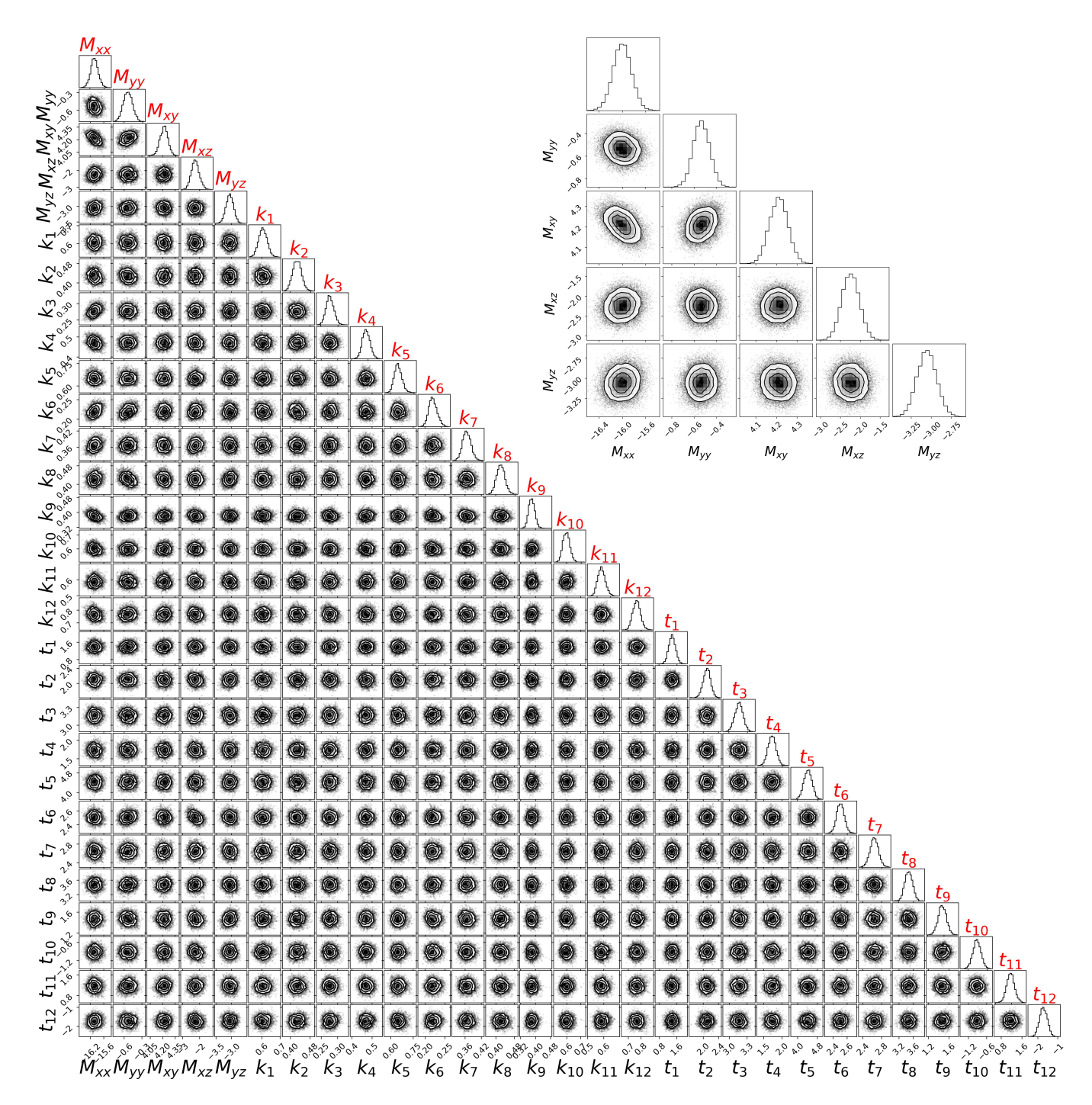


Figure 3 Posterior distribution of unknown parameters in the Bayesian MT inversion for the 2020 Zagreb earthquake (main-shock, Event 1), including five parameters of the deviatoric MT, M_{ij} 12 station-specific noise parameters, k_i , and 12 station-specific time shifts t_i . The unit of MT parameters is 5×10^{15} Nm. The unit of time shifts is a second. Noise parameters are unitless. Each subpanel shows a scatter plot of parameter pairs during the convergence stage of the inversion, with points shaded from black to gray according to density. The overlaid contours are included to highlight the shape of the distribution. A magnified view of five source parameters is shown in the upper right corner.

specific time shifts τ_i are also listed. The distribution of recovered time shifts is plotted in panel (a). The posterior distributions of the parameters are displayed in Figs. 3 and S2–S7, alongside the overlapping beachballs in Figs. 2 and 4–9 to illustrate the uncertainty in the solutions. The following sub-sections provide the details of the MT inversion results for each of the targeted earthquakes.

5.1 The three earthquakes in Croatia (mainland)

5.1.1 The 2020 Zagreb earthquake (mainshock)

Our inversion for the 2020 Zagreb earthquake (Event 1) reveals a pure DC mechanism of reverse faulting with a moment magnitude M_w 5.26 at a depth of 5 km (Fig. 2). The parameter search for source depth shows a clear peak at a depth of 5 km with the highest probability in Fig. 2(b). The mean MT from the convergence stage at

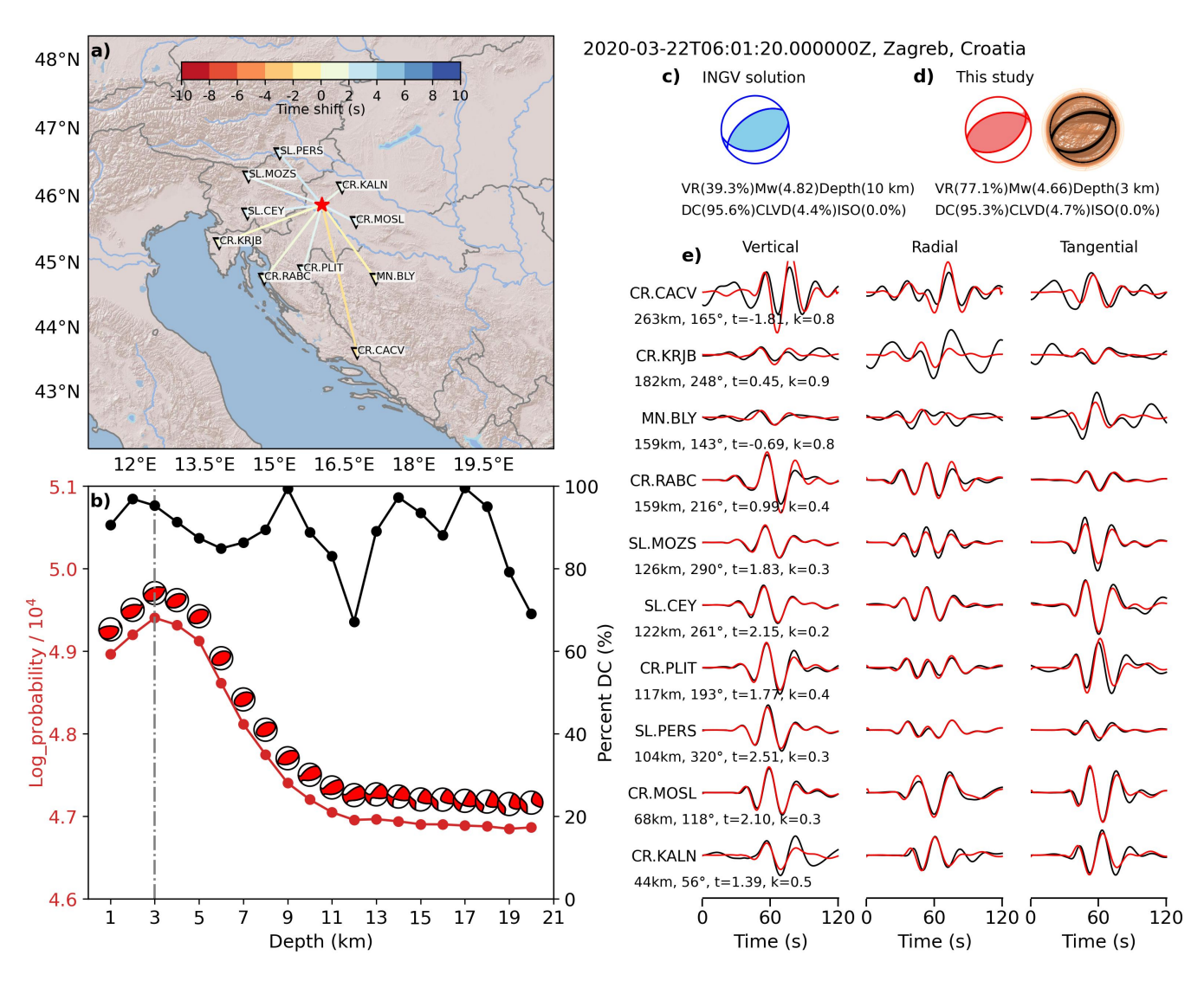


Figure 4 Inversion results for the largest aftershock of the 2020 Zagreb earthquake (Event 2). See the caption of Fig. 2 for details.

this optimal depth comprises a 97.8% DC and a 2.2% CLVD, as shown in Fig. 2(d). The focal mechanism indicates a reverse faulting with nodal planes defined in Table 2. This solution generates the predicted waveforms that fit the observations well, as evidenced by the variance reduction (VR) of 80%.

The posterior distribution of 29 inverted parameters, including 5 for the deviatoric MT, 12 for station-specific noise, and 12 for station-specific time shifts, is summarized in Fig. 3. A notable observation is that no multimodal distribution is observed for any parameter. Furthermore, the inter-parameter trade-off between each pair of parameters is negligible except for the pair of M_{xx} and M_{xy} , which shows a weak linear dependence in Fig. 3.

5.1.2 The largest aftershock of the 2020 Zagreb earthquake

The inversion results of the largest aftershock of the 2020 Zagreb earthquake (Event 2) in Fig. 4 suggest that the largest aftershock occurred shallow, at a depth of 3 km, with a similar focal mechanism to the mainshock. Our deviatoric MT inversion prefers a source dominated

by a 95.3% DC component and a negligible CLVD component (4.7%). The faulting has a geometry as listed in Table 2. The posterior distribution of 25 inverted parameters, including 5 for the deviatoric MT, 10 for station-specific noise, and 10 for station-specific time shifts, is summarized in Fig. S2. There is no multi-modal distribution observed in any of the parameters. Furthermore, there is no substantial inter-parameter tradeoff between each pair of parameters.

5.1.3 The largest foreshock of the 2020 Petrinja earthquake

The largest foreshock of the 2020 Petrinja earthquake was the M_L 4.9 event that struck on December 28, 2020, a day before the main M_w 6.4 earthquake. It occurred near the town of Petrinja, causing minor structural damage and alarming residents. The subsequent devastating mainshock caused significant destruction and casualties (e.g., Baize et al., 2022; Herak and Herak, 2023; Markušić et al., 2021). We exclude the mainshock in this study because further investigation may be needed to validate the point-source approximation for this event, given its larger magnitude. The MT inversion for its

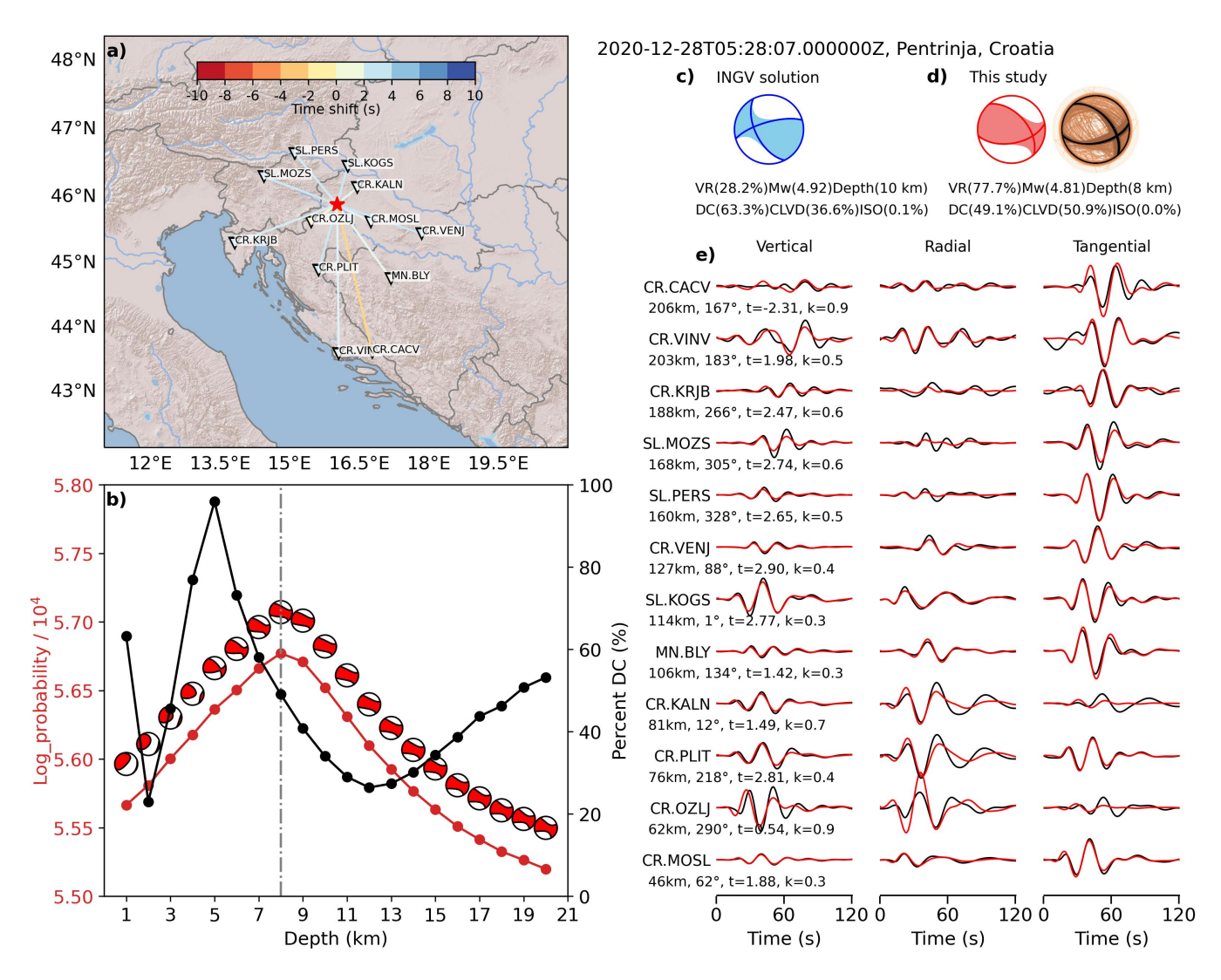


Figure 5 Inversion results for the largest foreshock of the 2020 Petrinja earthquake (Event 3). See the caption of Fig. 2 for details.

largest foreshock can contribute valuable insight into the source mechanism of the mainshock.

The inversion of full waveforms at 12 stations with very good azimuth coverage (Fig. 5a) indicates a significant non-DC mechanism during this earthquake. The parameter search for the source depth leads to a depth of 8 km with the highest probability, as shown in Fig. 5b. The MT solution at this optimal depth consists of 49.1% DC and 50.9% CLVD components. The nodal planes of the recovered DC solution are listed in Table 2. This source mechanism with the significant CLVD component can explain the observations at a fair waveform fit level with VR = 77.7% (Figs. 5d and 5e).

The posterior distribution of 29 inverted parameters, including 5 for the deviatoric MT, 12 for station-specific noise, and 12 for station-specific time shifts, can be found in Fig. S3. Similarly to previous cases, there is no multi-modal distribution for any of the parameters, and there is no substantial inter-parameter trade-off between each pair of parameters.

5.2 The two earthquakes in the offshore Adriatic Sea

For Event 4, our station-selection algorithm chooses eight stations, including one from Bosnia and Herzegovina, two from Croatia, and five from Italy, with a good azimuth coverage (ENS = 6.81) as in Fig. 6a. A parameter search for the source depth indicates that this earthquake occurred at a depth between 2 and 5 km where a very similar focal mechanism (as beachballs) and probability (the red curve) are obtained (Fig. 6b). The MT solutions at these depths indicate that the earthquake is a pure DC source because the CLVD component is very small which is close to zero for the depths of 4 km and 5 km as shown by the black curve in Fig. 6b. The optimal source depth is 4 km. The corresponding fault plane is included in Table 2.

The posterior distribution of 21 inverted parameters, including 5 for the deviatoric MT, 8 for station-specific noise, and 8 for station-specific time shifts, can be found in Fig. S4. Two stations, CR.DBRK and MN.BLY, require significant time shifts to align the predicted waveforms with the observations. Therefore, their time shift parameters, t_1 and t_8 , nearly saturate to the upper bound

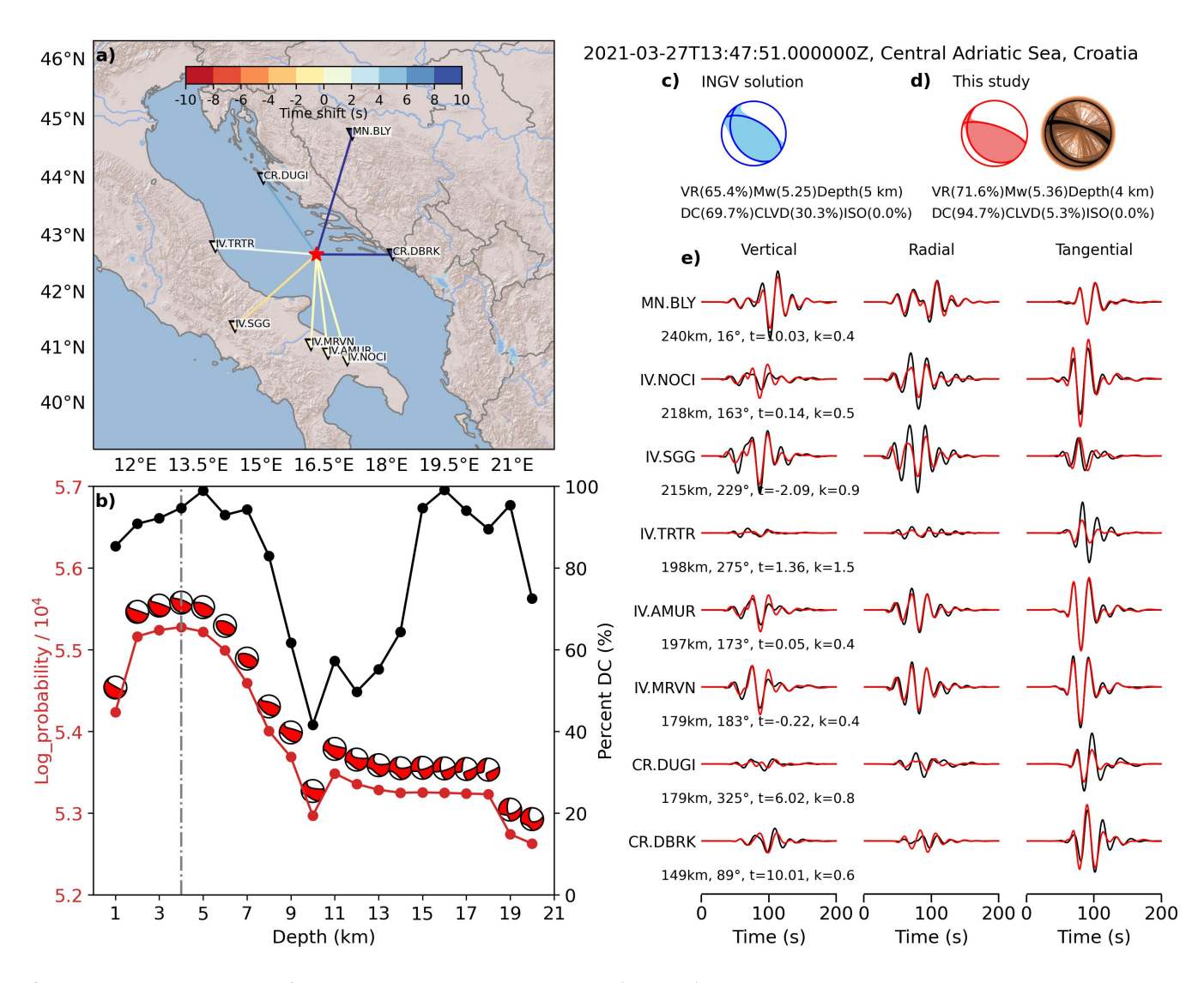


Figure 6 Inversion results for the central Adriatic earthquake (Event 4). The optimal source depth is 4 km. See the caption of Fig. 2 for details.

of the prior. The significant time shifts are likely because this event's actual location is about 30 km to the SSE from the location INGV used (last accessed on 10 October 2024; the location was updated in a recent work on this event by Di Luccio et al. (2025), which was under review during the time we prepared our manuscript).

For Event 5, we try to use the full waveforms but filter them into a shorter-period band, i.e., 15–50 s. We manually choose eight stations, as in Fig. 7a, because of the limited availability of stations on the regional scale considered. The azimuthal coverage is not as good as that of the other four events in Croatia. The inversion results are summarized in Fig. 7. The optimal source depth is 9 km, as shown in Fig. 7b, with a similar probability for 10 km. Our inversion suggests that this earthquake is a pure DC focal mechanism with a 96.8% DC component and a negligible CLVD component (3.2%). The nodal planes of the focal mechanism are listed in Table 2. The posterior distribution of 21 inverted parameters can be found in Fig. S5. No multi-modal distributions and no substantial inter-parameter trade-offs were observed.

5.3 The two earthquakes in Italy

For Event 6, our inversion favors a DC-dominated source together with a large CLVD component mechanism (Fig. 8). The station-selection algorithm chooses eight stations with a good azimuthal coverage of ENS = 6.57 as in Fig. 8a. The search for the optimal source depth results in a depth of 6 km. As shown in Fig. 8c, our deviatoric MT solution consists of dominating DC (78.1%) and significant CLVD (21.9%) components. The solutions support reverse faulting during this earthquake with nodal planes listed in Table 2. We obtain a moment magnitude $M_w = 5.5$. The posterior distribution of 21 inverted parameters in Fig. S6 demonstrates that no multi-modal distributions and no strong interparameter trade-offs are observed.

The inversions for Event 7 are summarized in Fig. 9. Our algorithm chooses eight stations with a high azimuthal coverage of ENS = 7.8 as plotted in Fig. 9a. The parameter search for the source depth leads to a depth of 3 km, as shown by the red curve in Fig. 9b. As listed in Table 2 and Fig. 9d, our MT solution includes a significant DC component (87.3%) and a 12.7% CLVD component. The DC component indicates a normal faulting

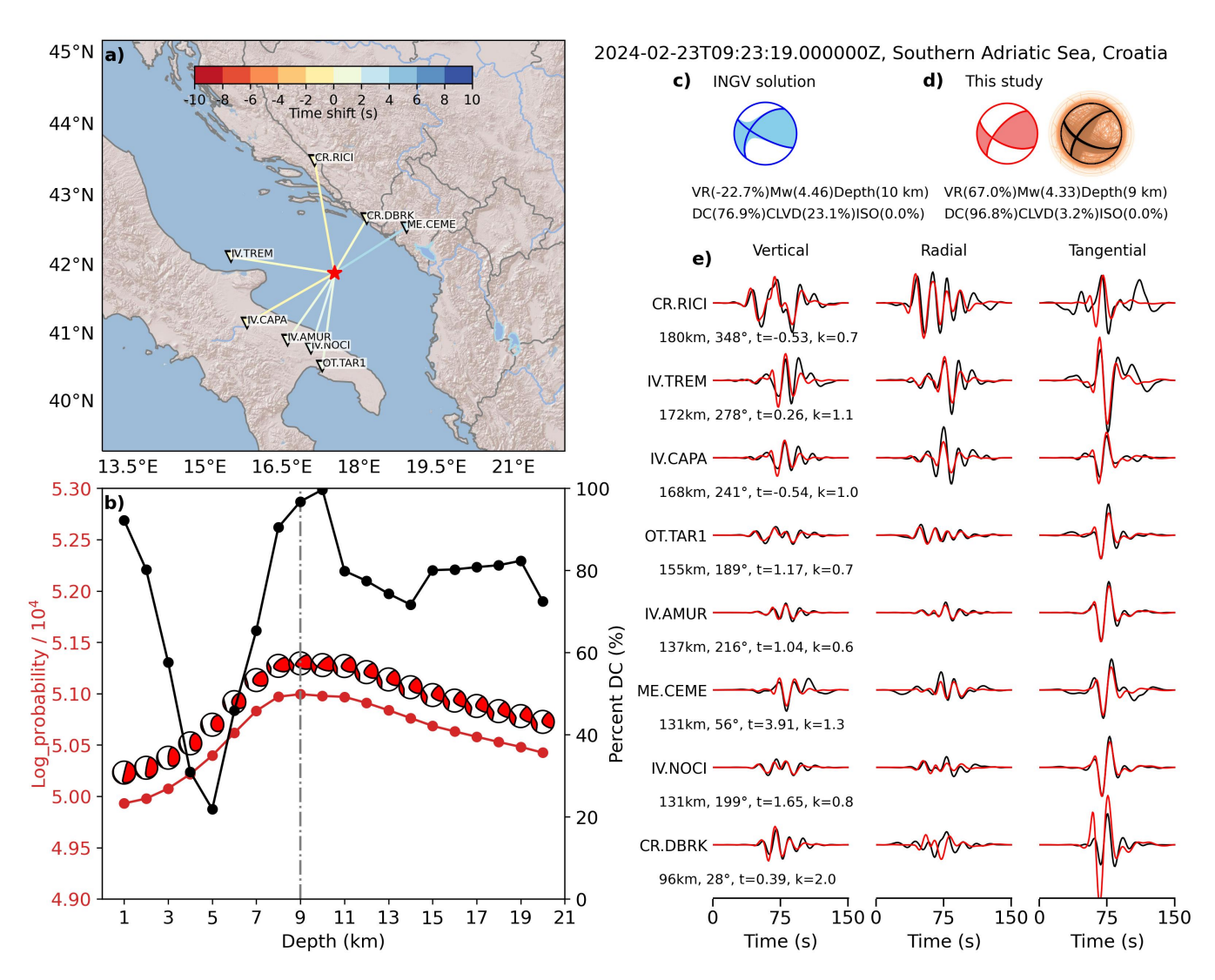


Figure 7 Inversion results for the southern Adriatic earthquake (Event 5). The optimal source depth is 9 km. See the caption of Fig. 2 for details.

with nodal planes in Table 2. The predicted waveforms from our deviatoric MT match with the observations at a high level of VR = 89.7%. The posterior distribution of 21 inverted parameters can be found in Fig. S7. No multimodal distributions were observed. However, the linear dependency between MT parameters and noise or time shift parameters is present.

6 Discussion

6.1 The presence of non-DC components

We investigate the notable presence of a CLVD component in the MT solutions for three earthquakes—Event 3, Event 6, and Event 7—with particular emphasis on Event 3, which includes a 50.9% CLVD component. First, we perform a full MT inversion using the optimal source depth determined from the previous depth search. As shown in Fig. 10, the full MT inversion for Event 3 yields significant non-DC components: 50.4% CLVD and 5.0% ISO, consistent with the deviatoric MT inversion results presented in Section 5.1.3.

We conduct a jackknife sensitivity test to assess the robustness of the inversion results, particularly the sub-

stantial CLVD component. In this test, we randomly discard 1 to 5 of the 12 stations and repeat the deviatoric MT inversion 8 times for each case, resulting in 40 inversions at a depth of 8 km. As shown in Fig. S8, the CLVD component remains consistently present in all solutions, with a mean value of 50.1%. Given the regional tectonic setting, volcanic and geothermal contributions to the large CLVD component can be excluded. Although the liquefaction was observed during the mainshock (i.e., the 2022 M_w 6.4 Petrinja earthquake), possible fluid effects at the source depth is unlikely to contribute to the CLVD component. Instead, the complex aftershock sequence of the mainshock (Herak and Herak, 2023) suggested it may reflect the geometric complexity of the source process likely involving two or more nearby faults.

Similarly, the full MT inversions and sensitivity tests for Event 6 (Figs. S9 and S10) and Event 7 (Figs. S11 and S12) confirm the presence of CLVD components in their solutions. We performed a series of inversions by randomly removing one station from the selected 8 stations (8 trials), then repeated the process with removal of 2 and 3 stations, resulting in a total of 24 inversions. The sensitivity tests obtain an average CLVD component of

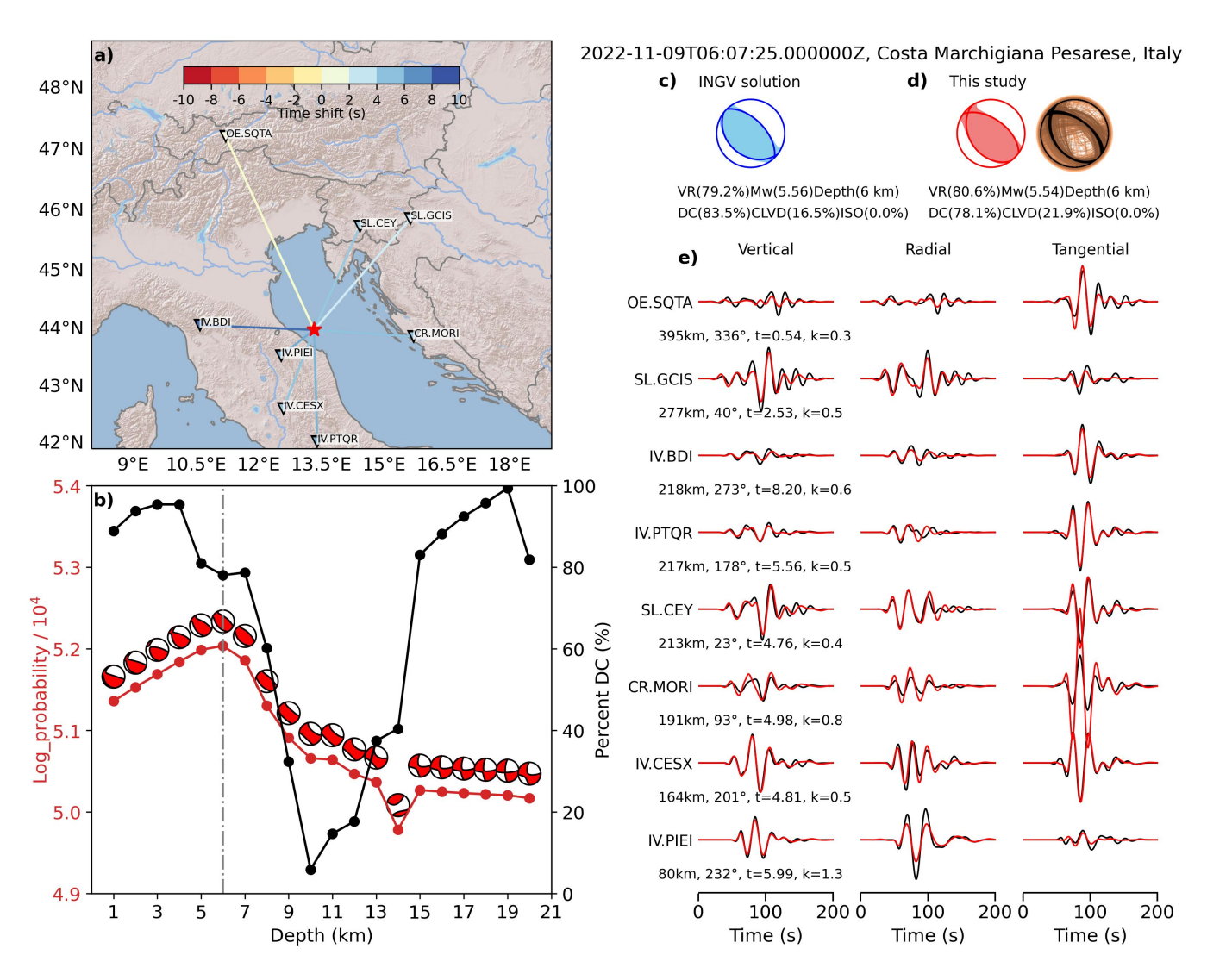


Figure 8 Inversion results for the 2022 M_w 5.5 earthquake in Costa Marchigiana Pesarese (Event 6). The optimal source depth is 6 km. See the caption of Fig. 2 for details.

21.6% for Event 6 and 21.3% for Event 7, even though the values fluctuate likely due to the decreased azimuthal coverage after discarding 1–3 stations from the original set of 8 stations shown in Figs. 8a and 9a. However, the underlying causes of the non-DC components in these three events remain uncertain and warrant further investigation, which is beyond the scope of this study. Nonetheless, the presence of the CLVD component is consistent with the INGV solutions, albeit with varying degrees of significance. Notably, our solution for Event 3, which includes a higher CLVD component, provides a better fit to the observed data than the INGV solution.

6.2 Comparison with solutions from available routine catalogs

For Event 1, compared with the INGV solution, which includes a significant CLVD component of up to 32.3%, our pure DC solution is 1 km shallower and provides a much higher VR (by 12%) using the GFs under the same source-station configuration but taking its own depth, as shown in Figs. 2c–2e. The Kagan angle (Kagan, 1991; Tape and Tape, 2012) expressing the angular distance between our solution and the INGV solution is

11°. The fault geometry angles obtained here exceed the range of the HRCS038 seismogenic fault from the European Database of Seismogenic Faults (Basili et al., 2013), which expects a $50^{\circ}-60^{\circ}$ strike, $50^{\circ}-70^{\circ}$ dip, and $20^{\circ}-50^{\circ}$ rake. However, they are consistent with the solution of [strike = 67° , dip = 47° , rake = 79°] or [strike = 263° , dip = 44° , rake = 102°] from the inversion of first motion polarity data by Herak et al. (2021b).

The solution of Event 2, the largest aftershock of the 2020 Zagreb earthquake, is very similar to the mainshock with a Kagan angle of 11°, but shows a small difference from the INGV solution of [strike = 78°, dip = 38° , rake = 108°] or [strike = 235° , dip = 54° , rake = 76°] with a Kagan angle of 21°. Even though both our and INGV solutions favor pure DC sources, our MT solution generates a much better waveform fit (VR = 77.1% vs. VR = 39.3%) between the observations and predictions at eight chosen stations, as shown in Figs. 4c-4e. The source of difference in waveform fit could be the deeper source depth (10 km) and a higher moment magnitude in the INGV solution. We may have a better constraint on the source depth and the magnitude by incorporating uncertainty treatment using a composite Earth model (Fig. S1) and incorporating more local stations

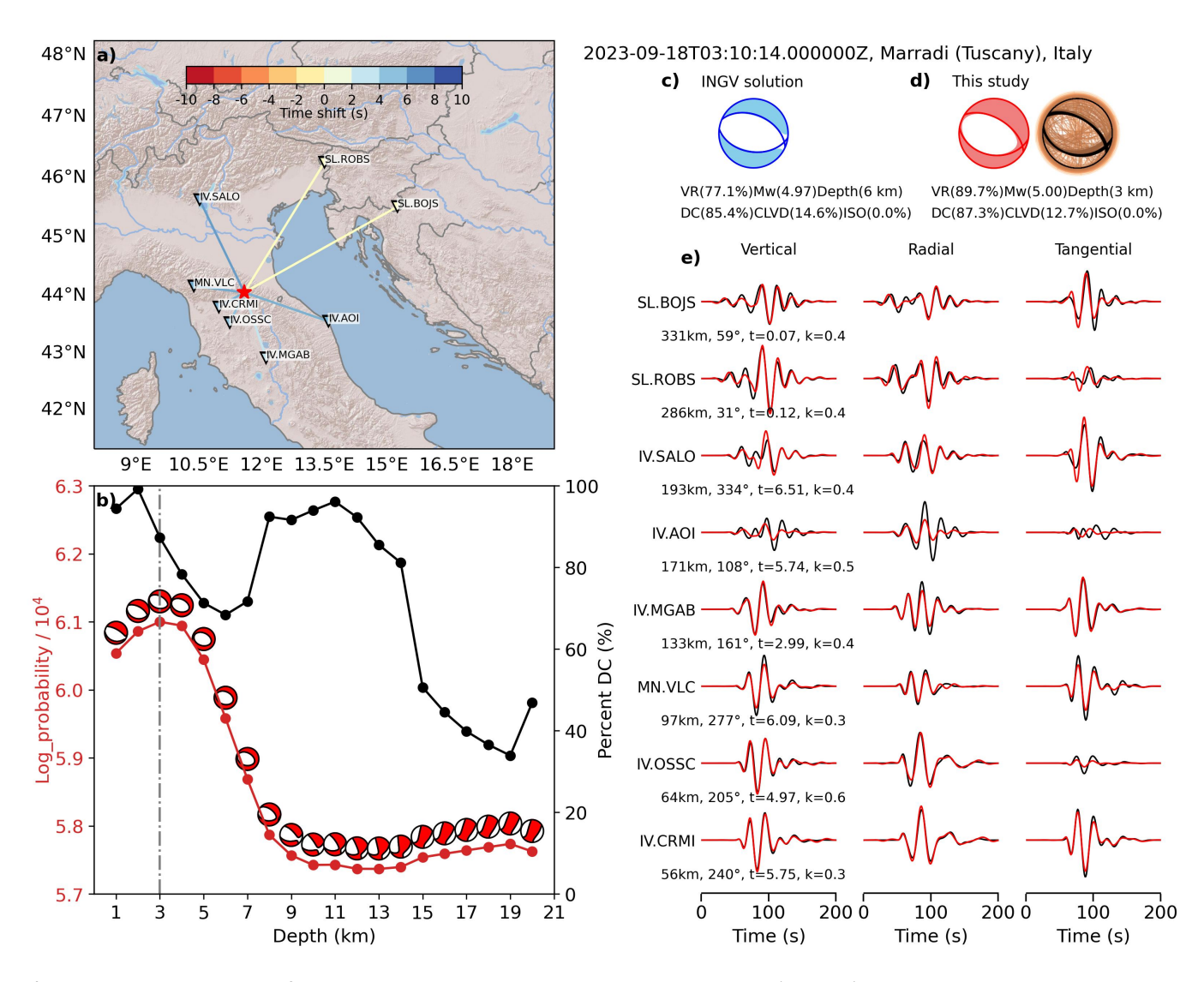


Figure 9 Inversion results for the 2023 M_w 4.9 earthquake in Marradi, Tuscany (Event 7). The optimal source depth is 3 km. See the caption of Fig. 2 for details.

(Fig. 4a).

The recovered faulting for Event 3 is expected by the HRCS37 seismogenic fault model (Basili et al., 2013), which predicts a 60°-80° strike, 50°-70° dip, and 20°-50° rake. Similarly, the INGV solution for this event also favors a non-DC source with 63.3% DC and 36.6% CLVD components. However, the focal mechanism is significantly different in the INGV catalog [strike = 254°, dip = 72°, rake = 34°] or [strike = 153°, dip = 58°, rake = 159°] with a Kagan angle of 88°, as plotted in Fig. 5c, and their solution can only fit part of the data considered here, with a relatively low VR of only 28.2%. The focal mechanism obtained here is also different from the solutions [strike = 335° , dip = 85° , rake = -179°] or [strike = 245° , $dip = 89^{\circ}$, rake = -4°] from Herak and Herak (2023) using the first motion polarity data and assuming a pure DC source mechanism.

For Event 4, we obtain a source depth of 4 km, which is consistent with the 5 km depth reported in the INGV solution, despite the latter including a significant CLVD component of up to 30%. The geometry of the fault is similar to the INGV solution (Kagan angle of 18°) as plotted in Fig. 6c, as both solutions support a re-

verse faulting for this event. The estimated moment magnitude M_w = 5.36, at the optimal depth of 4 km is 0.11 larger than the one from INGV. Our solution produces a better waveform fit between the observations and predictions at these eight stations, as shown in Fig. 6d and 6e.

For Event 5, our inversion indicates a pure DC focal mechanism, while the INGV solution in Fig. 7c has a much higher CLVD component of 23.1%. Additionally, our estimated magnitude is smaller than the INGV's estimate. The Kagan angle between them is 20°. These differences lead to a much better waveform fit to the used observations than the INGV solution, as in Fig. 7c–7e. The focal mechanism in this study is also somewhat different than the ones from the first motion polarity data (Herak, 2024) [strike = 113°, dip = 65°, rake = 170°] or [strike = 207°, dip = 81°, rake = 25°]. They both depict a strike-slip mechanism but rotated slightly relative to each other (Kagan angle of 23°). The obtained source depth of 9 km agrees with the 10 km from the INGV solution.

For Event 6, both our solution and the INGV solution support the reverse faulting with similar nodal planes as

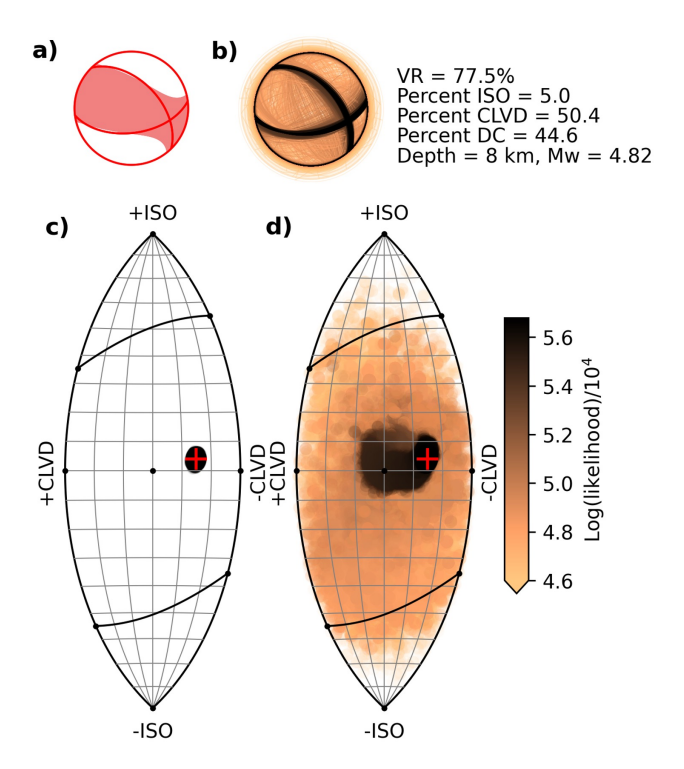


Figure 10 Full MT inversion results for Event 3. (a) Beachball of the mean MT solution. (b) Beachballs of all MT solutions sampled throughout the entire inversion process, color-coded by the logarithm of the likelihood (see color bar on the right). (c) Lune diagram showing MTs from the converged stage of the inversion; the red cross marks the mean solution. (d) Lune diagram showing the evolution of MTs over the whole inversion stage, with each solution colored by its log-likelihood, consistent with panel (b).

listed in Table 2 and in Figs. 8c and 8d with a Kagan angle of 13°. We obtain the same source depth of 6 km and a similar moment magnitude, $M_w=5.5$, as the INGV because both methods use the same velocity model (CIA model) and similar regional waveforms. The MT solutions in this study and those from the INGV catalog generate the same waveform fit between the observations and predictions (Figs. 8c–8e). However, a difference between them is still observed; a CLVD component obtained here is 5% larger than the INGV result.

For Event 7, we obtained a shallower source depth, 3 km, compared to the 6 km depth from the INGV catalog, but the MT solutions are similar, with a Kagan angle of 11°, both dominated by a DC component with a large CLVD component. Both solutions indicate normal faulting with comparable nodal planes. The predicted waveforms from our deviatoric MT show a higher level of agreement with the observed data (VR = 89.7%), which is 12% higher than that of the INGV solution (Figs. 9c-9e). Such a good waveform fit could be caused by the shallower source depth, which not only corresponds to the highest probability (see Fig. 9b), but also yields the near-highest VR among the tested depths for this event (VRs for 1–6 km are 86.0%, 88.0%, 89.7%, 90.0%, 87.5%, and 81.2%, respectively).

In the case of Event 7, more linear dependencies between parameters are observed in Fig. S7, such as be-

tween M_{xz} and M_{yz} , as well as between M_{yz} and t_1 , t_3 , t_4 , etc. Their underlying causes remain uncertain. A plausible explanation is the decreased resolution associated with shallow events, since such similar dependencies are not observed for the deeper events (e.g., Events 1, 3, 5, and 6). Additionally, the presence of significant non-DC components in its MT solution likely increases the effect of model complexity, making it different from the other shallow events at similar depths, such as Events 2 and 4.

6.3 Challenge for small events

For Event 5, the full waveform inversion is challenging because its magnitude is smaller than other events in this study. This earthquake occurred in the south Adriatic basin—the deepest part of the Adriatic Sea. Unlike other regions of the Adriatic Sea, this area rarely experiences seismicity, according to the Croatian Earthquake Catalogue (Herak et al., 1996), with supplemented data up to 2022. The INGV reported a local magnitude of M_L 4.7 for this unexpected earthquake. Based on the empirical relationship between the duration and the moment magnitude (Ekström et al., 1992; Ekström and Engdahl, 1989), the ruptures of smaller earthquakes usually last shorter, and are therefore more efficient at generating high-frequency waveforms. The resolvability of source parameters for smaller earthquakes relies on the use of shorter-period full waveform data but remains difficult because of the simplified description of the Earth's structures, as discussed in our previous studies (e.g., Hu et al., 2023; Pham et al., 2024). Alternatively, utilizing the parts of full waveforms, such as the first motion polarity, the amplitudes, or amplitude ratios, can mitigate the demanding high-frequency waveform modeling. A detailed summary can be found in Shang and Tkalčić (2020).

6.4 Station-specific time shifts as measures of structural error

The station-specific time shifts between the observations and predictions and station-specific noise for the mainshock and aftershock of the 2020 Zagreb earthquake (Events 1 and 2) exhibit a consistent pattern. As shown in Fig. S13a, the common stations used for both events require similar time shifts to re-align the predicted waveforms with the observations. This consistency arises because the time shifts are primarily due to the structural error in the Earth model. Consequently, the spatial distribution of these shifts reflects regional structural heterogeneity, as discussed by Hu et al. (2023). Furthermore, the estimated relative noise levels at the stations are also consistent between the two earthquakes, as illustrated in Fig. S13b.

A key distinction in our MT inversion approach lies in handling uncertainty related to structural errors and data noise, which largely accounts for the differences between our MT solutions and those reported in existing earthquake catalogs. Structural errors are addressed through station-specific time shifts between the observed and predicted waveforms. Unlike the cut-andpaste (CAP) method (Zhao and Helmberger, 1994; Zhu

and Helmberger, 1996), these time shifts are treated as free parameters, allowing us to fully account for their uncertainty. On the other hand, data noise is assumed to be uncorrelated, modelled using a diagonal covariance matrix in Eq. 1), justified by the high SNRs observed in most events. Hu et al. (2023) highlighted the importance of this assumption for inverting small to moderate earthquakes. Although incorporating correlated noise, as done by Mustać and Tkalčić (2016), can be beneficial, it requires a full covariance matrix and is computationally intensive. This study proposes a lightweight alternative with discussed assumptions, offering a practical solution for developing a modern earthquake catalog in this region.

7 Conclusions

In this study, we utilize our evolving Bayesian MT inversion to determine MT parameters for seven earthquakes with reported magnitudes between 4.5 and 5.5 over the past five years in the Adriatic Sea and its surrounding areas in Croatia and Italy. The method considers the uncertainty deriving from data noise and structural errors due to the simplified description of Earth's interior. The optimal source depths, mean MT solutions, their decompositions, corresponding nodal planes, and associated uncertainties for the seven earthquakes are summarized in Tables 1 and 2. Our results show that four events (Event 1, Event 2, Event 4, and Event 5 in Table 1) exhibit nearly pure DC mechanisms. The remaining three events show significant non-DC components: Event 3 has a significant CLVD component of 50.9%, whereas Event 6 and Event 7 have smaller but consistent CLVD components (21.95% and 12.7%, respectively). In addition, Event 2 and Event 7 have shallow optimal source depths of 3 km.

The comparison with the INGV and other regional catalogs demonstrates the method's feasibility and potential improvement in source determination after uncertainty treatment for data noise and structural error. Our MT solutions for Event 6 and Event 7 in Italy closely match those from INGV, likely due to the use of the same velocity model and similar network coverage. For Event 2, we obtained a shallower source depth of 3 km than 10 km from INGV by using different velocity models, even though both solutions support a similar pure-DC mechanism. For Event 3, both our solution and that of INGV include significant non-DC components, the origins of which warrant further investigation. In contrast, our pure-DC solutions for Events 1, 4, and 5 differ from the INGV solution with significant non-DC components and can better fit the waveforms selected by a stationselection scheme considering epicenter distance, SNR, and azimuth coverage. The refined source mechanisms could complement local seismogenic fault models for the complex geological setting, assess the hazard potential, and support improvement to the regional earthquake catalogs in the Adriatic Sea region.

Acknowledgments

The authors thank the handling editor Wenbin Xu and the two reviewers, Jan Šíleny and Angela Sarao, for their thoughtful reviews and constructive feedback. This research was undertaken with the assistance of resources from the National Computational Infrastructure (NCI Australia) (em78), an NCRIS-enabled capability supported by the Australian Government. H.T. thanks the Australian Research Council and US DoD for their continuing support of earthquake source physics research. T.-S. P. acknowledges financial support from the Australian Research Council through a Discovery Early Career Researcher Award, project DE230100025.

Data and Code Availability

Data for three earthquakes occurring in Croatian (land) are mainly from the local network in Croatia, the Croatian Seismograph Network (University of Zagreb, 2001). For further inquiries about this part of the data, contact Iva Dasović (dasovici@gfz.hr). Other data for this study are freely downloaded from the European Integrated Data Archive (https://orfeus-eu.org/data/eida/) in Observatories and Research Facilities for European Seismology (ORFEUS). We use stations from Seismic Network of the Republic of Slovenia: identifier SL (Slovenian Environment Agency, 1990), Mediterranean Very Broadband Seismographic Network: identifier MN (MedNet Project Partner Institutions, 1990), AlpArray: identifier Z3 (AlpArray Seismic Network, 2015), Italian National Seismic Network: identifier IV (Istituto Nazionale di Geofisica e Vulcanologia (INGV), 2005), Montenegrin Seismic Network: identifier ME (Sector for Seismology, Institute of Hydrometeorology and Seismology of Montenegro, 1982), OTRIONS: identifier OT (University of Bari "Aldo Moro", 2013), and Austrian Seismic Network: identifier OE (Z.A.M.G. Zentralanstalt für Meterologie und Geodynamik, 1987). INGV's origin time, location, and MT solutions are accessed from the updated version of Pondrelli (2002) at http://rcmt2.bo.ingv.it/ (last accessed on 10 October 2024). Figures were made with Matplotlib (Hunter, 2007), and the scattering posterior plots were plotted with corner (Foreman-Mackey, 2016). Seismic data was analyzed with Obspy (Beyreuther et al., 2010). Our method uses a Bayesian sampler from a welltested Python package, emcee (Foreman-Mackey et al., 2013).

Competing interests

The authors declare no conflict of interest.

References

Albini, P. *The Great 1667 Dalmatia Earthquake: An In-Depth Case Study.* Springer International Publishing, 2015. doi: 10.1007/978-3-319-16208-9.

AlpArray Seismic Network. AlpArray Seismic Network (AASN) temporary component, 2015. doi: 10.12686/alparray/z3_2015. [Dataset].

- Alvizuri, C. and Tape, C. Full Moment Tensor Analysis of Nuclear Explosions in North Korea. Seismological Research Letters, 89 (6):2139–2151, Sept. 2018. doi: 10.1785/0220180158.
- Atalić, J., Uroš, M., Šavor Novak, M., Demšić, M., and Nastev, M. The Mw5.4 Zagreb (Croatia) earthquake of March 22, 2020: impacts and response. *Bulletin of Earthquake Engineering*, 19(9): 3461–3489, May 2021. doi: 10.1007/s10518-021-01117-w.
- Baize, S., Amoroso, S., Belić, N., Benedetti, L., Boncio, P., Budić, M., Cinti, F. R., Henriquet, M., Jamšek Rupnik, P., Kordić, B., Markušić, S., Minarelli, L., Pantosti, D., Pucci, S., Špelić, M., Testa, A., Valkaniotis, S., Vukovski, M., Atanackov, J., Barbača, J., Bavec, M., Brajkovič, R., Brčić, V., Caciagli, M., Celarc, B., Civico, R., De Martini, P. M., Filjak, R., Iezzi, F., Moulin, A., Kurečić, T., Métois, M., Nappi, R., Novak, A., Novak, M., Pace, B., Palenik, D., and Ricci, T. Environmental effects and seismogenic source characterization of the December 2020 earthquake sequence near Petrinja, Croatia. *Geophysical Journal International*, 230 (2):1394–1418, Mar. 2022. doi: 10.1093/gji/ggac123.
- Basili, R., Kastelic, V., Demircioglu Tumsa, M. B., Garcia Moreno, D.,
 Nemser, E. S., Petricca, P., Sboras, S. P., Besana-Ostman, G. M.,
 Cabral, J., Camelbeeck, T., Caputo, R., Danciu, L., Domaç, H.,
 Fonseca, J. F. d. B. D., García-Mayordomo, J., Giardini, D., Glavatovic, B., Gulen, L., Ince, Y., Pavlides, S., Sesetyan, K., Tarabusi,
 G., Tiberti, M. M., Utkucu, M., Valensise, G., Vanneste, K., Vilanova, S. P., and Wössner, J. European Database of Seismogenic Faults (EDSF), 2013. doi: 10.6092/INGV.IT-SHARE-EDSF.
- Beyreuther, M., Barsch, R., Krischer, L., Megies, T., Behr, Y., and Wassermann, J. ObsPy: A Python Toolbox for Seismology. *Seismological Research Letters*, 81(3):530–533, May 2010. doi: 10.1785/gssrl.81.3.530.
- Chiarabba, C., Jovane, L., and DiStefano, R. A new view of Italian seismicity using 20 years of instrumental recordings. *Tectonophysics*, 395(3–4):251–268, Jan. 2005. doi: 10.1016/j.tecto.2004.09.013.
- Di Luccio, F., Palano, M., Scognamiglio, L., Marchetti, A., Dasović, I., Mustać, M., Magnoni, F., Harris, P. A., Casarotti, E., Polonia, A., Gasperini, L., Dannowski, A., and Kopp, H. The Role of Salt Tectonics in the 2021 Central Adriatic Seismic Sequence. *Earth and Space Science*, 12(5), Apr. 2025. doi: 10.1029/2025ea004216.
- Dreger, D. S., Tkalčić, H., and Johnston, M. Dilational Processes Accompanying Earthquakes in the Long Valley Caldera. *Science*, 288(5463):122–125, Apr. 2000. doi: 10.1126/science.288.5463.122.
- Duputel, Z., Rivera, L., Fukahata, Y., and Kanamori, H. Uncertainty estimations for seismic source inversions: Uncertainty estimations for source inversions. *Geophysical Journal International*, 190(2):1243–1256, June 2012. doi: 10.1111/j.1365-246x.2012.05554.x.
- D'Agostino, N., Avallone, A., Cheloni, D., D'Anastasio, E., Mantenuto, S., and Selvaggi, G. Active tectonics of the Adriatic region from GPS and earthquake slip vectors. *Journal of Geophysical Research: Solid Earth*, 113(B12), Dec. 2008. doi: 10.1029/2008jb005860.
- Ekström, G. Global Detection and Location of Seismic Sources by Using Surface Waves. *Bulletin of the Seismological Society of America*, 96(4A):1201–1212, Aug. 2006. doi: 10.1785/0120050175.
- Ekström, G. and Engdahl, E. R. Earthquake source parameters and stress distribution in the Adak Island region of the central Aleutian Islands, Alaska. *Journal of Geophysical Research: Solid Earth*, 94(B11):15499–15519, Nov. 1989. doi: 10.1029/jb094ib11p15499.
- Ekström, G., Stein, R. S., Eaton, J. P., and Eberhart-Phillips, D. Seismicity and geometry of a 110-km-long blind thrust fault 1. The

- 1985 Kettleman Hills, California, earthquake. *Journal of Geophysical Research: Solid Earth*, 97(B4):4843–4864, Apr. 1992. doi: 10.1029/91jb02925.
- Foreman-Mackey, D. corner.py: Scatterplot matrices in Python. *The Journal of Open Source Software*, 1(2):24, June 2016. doi: 10.21105/joss.00024.
- Foreman-Mackey, D., Hogg, D. W., Lang, D., and Goodman, J. emcee: The MCMC Hammer. *Publications of the Astronomical Society of the Pacific*, 125(925):306–312, Mar. 2013. doi: 10.1086/670067.
- Govorčin, M., Herak, M., Matoš, B., Pribičević, B., and Vlahović, I. Constraints on Complex Faulting during the 1996 Ston–Slano (Croatia) Earthquake Inferred from the DInSAR, Seismological, and Geological Observations. *Remote Sensing*, 12(7):1157, Apr. 2020. doi: 10.3390/rs12071157.
- Halauwet, Y., Afnimar, Triyoso, W., Vackář, J., Daryono, D., Supendi, P., Daniarsyad, G., Simanjuntak, A. V. H., Pranata, B., Narwadan, H. A. A. M., and Hakim, M. L. A new automated procedure to obtain reliable moment tensor solutions of small to moderate earthquakes (3.0 ≤ M ≤ 5.5) in the Bayesian framework. *Geophysical Journal International*, 239(2):1000–1020, Aug. 2024. doi: 10.1093/gji/ggae309.
- Hallo, M. and Gallovič, F. Fast and cheap approximation of Green function uncertainty for waveform-based earthquake source inversions. *Geophysical Journal International*, 207(2):1012–1029, Aug. 2016. doi: 10.1093/gji/ggw320.
- Handy, M. R., M. Schmid, S., Bousquet, R., Kissling, E., and Bernoulli, D. Reconciling plate-tectonic reconstructions of Alpine Tethys with the geological–geophysical record of spreading and subduction in the Alps. *Earth-Science Reviews*, 102(3–4): 121–158, Oct. 2010. doi: 10.1016/j.earscirev.2010.06.002.
- Hantken von Prudnik, M. Das Erdbeben von Agram im Jahre 1880, 1882. Mittheilungen aus dem Jahrbuche der Kon. Ungarischen Geologischen Anstalt, Budapest, Gebruder Legrady, (in German).
- Herak, D. and Herak, M. Veliki zagrebački potres 1880. *Meridijani*, 109:24–33, 2006.
- Herak, D., Herak, M., Prelogović, E., Markušić, S., and Markulin, Ž. Jabuka island (Central Adriatic Sea) earthquakes of 2003. *Tectonophysics*, 398(3–4):167–180, Apr. 2005. doi: 10.1016/j.tecto.2005.01.007.
- Herak, D., Herak, M., and Tomljenović, B. Seismicity and earthquake focal mechanisms in North-Western Croatia. *Tectonophysics*, 465(1–4):212–220, Feb. 2009. doi: 10.1016/j.tecto.2008.12.005.
- Herak, D., Herak, M., and Vrkić, I. The Earthquake of 13 April 1850 near Ston, Croatia: Macroseismic Analyses. *Seismological Research Letters*, 95(2A):1043–1056, Nov. 2023. doi: 10.1785/0220230299.
- Herak, M. Croatian catalogue and database of focal mechanism solutions, characteristic mechanisms, and stress field properties in the Dinarides and the surrounding regions. *Geofizika*, 41 (2):79–123, Jan. 2024. doi: 10.15233/gfz.2024.41.5.
- Herak, M. and Herak, D. Properties of the Petrinja (Croatia) earthquake sequence of 2020–2021 – Results of seismological research for the first six months of activity. *Tectonophysics*, 858: 229885, July 2023. doi: 10.1016/j.tecto.2023.229885.
- Herak, M. and Herak, D. A Comparative Study of Building Damage in Ston, Croatia, Caused by the Earthquakes of 1850 and 1996. Seismological Research Letters, 95(5):3070–3081, July 2024. doi: 10.1785/0220240248.
- Herak, M., Herak, D., and Markušić, S. Revision of the earthquake catalogue and seismicity of Croatia, 1908–1992. *Terra Nova*, 8

- (1):86-94, Jan. 1996. doi: 10.1111/j.1365-3121.1996.tb00728.x.
- Herak, M., Herak, D., and Orlić, N. Properties of the Zagreb 22 March 2020 earthquake sequence: analyses of the full year of aftershock recording. *Geofizika*, 38(2):93–116, Jan. 2021a. doi: 10.15233/gfz.2021.38.6.
- Herak, M., Herak, D., and Živčić, M. Which one of the three latest large earthquakes in Zagreb was the strongest the 1905, 1906 or the 2020 one? *Geofizika*, 38(2):117–146, Jan. 2021b. doi: 10.15233/gfz.2021.38.5.
- Herrmann, R. B. Computer Programs in Seismology: An Evolving Tool for Instruction and Research. *Seismological Research Letters*, 84(6):1081–1088, Oct. 2013. doi: 10.1785/0220110096.
- Herrmann, R. B., Malagnini, L., and Munafo, I. Regional Moment Tensors of the 2009 L'Aquila Earthquake Sequence. *Bulletin of the Seismological Society of America*, 101(3):975–993, May 2011. doi: 10.1785/0120100184.
- Hu, J., Phạm, T.-S., and Tkalčić, H. Seismic moment tensor inversion with theory errors from 2-D Earth structure: implications for the 2009–2017 DPRK nuclear blasts. *Geophysical Journal International*, 235(3):2035–2054, Sept. 2023. doi: 10.1093/gji/ggad348.
- Hu, J., Phạm, T., and Tkalčić, H. A Composite Seismic Source Model for the First Major Event During the 2022 Hunga (Tonga) Volcanic Eruption. *Geophysical Research Letters*, 51(18), Sept. 2024. doi: 10.1029/2024gl109442.
- Hunter, J. D. Matplotlib: A 2D Graphics Environment. Computing in Science & Engineering, 9(3):90–95, 2007. doi: 10.1109/m-cse.2007.55.
- Istituto Nazionale di Geofisica e Vulcanologia (INGV). Rete Sismica Nazionale (RSN), 2005. doi: 10.13127/sd/x0fxnh7qfy. [Dataset].
- Ivančić, I., Herak, D., Herak, M., Allegretti, I., Fiket, T., Kuk, K., Markušić, S., Prevolnik, S., Sović, I., Dasović, I., and Stipčević, J. Seismicity of Croatia in the period 2006-2015. *Geofizika*, 35 (1):69–98, 2018. doi: 10.15233/gfz.2018.35.2.
- Jost, M. L. and Herrmann, R. B. A Student's Guide to and Review of Moment Tensors. Seismological Research Letters, 60(2):37–57, Apr. 1989. doi: 10.1785/gssrl.60.2.37.
- Julian, B. R., Miller, A. D., and Foulger, G. R. Non-double-couple earthquakes 1. Theory. *Reviews of Geophysics*, 36(4):525–549, Nov. 1998. doi: 10.1029/98rg00716.
- Kagan, Y. Y. 3-D rotation of double-couple earthquake sources. Geophysical Journal International, 106(3):709–716, Sept. 1991. doi: 10.1111/j.1365-246x.1991.tb06343.x.
- Kastelic, V., Vannoli, P., Burrato, P., Fracassi, U., Tiberti, M. M., and Valensise, G. Seismogenic sources in the Adriatic Domain. *Marine and Petroleum Geology*, 42:191–213, Apr. 2013. doi: 10.1016/j.marpetgeo.2012.08.002.
- Knopoff, L. and Randall, M. J. The compensated linear-vector dipole: A possible mechanism for deep earthquakes. *Journal* of *Geophysical Research*, 75(26):4957–4963, Sept. 1970. doi: 10.1029/jb075i026p04957.
- Latorre, D., Di Stefano, R., Castello, B., Michele, M., and Chiaraluce, L. An updated view of the Italian seismicity from probabilistic location in 3D velocity models: The 1981–2018 Italian catalog of absolute earthquake locations (CLASS). *Tectonophysics*, 846: 229664, Jan. 2023. doi: 10.1016/j.tecto.2022.229664.
- Le Breton, E., Handy, M. R., Molli, G., and Ustaszewski, K. Post-20 Ma Motion of the Adriatic Plate: New Constraints From Surrounding Orogens and Implications for Crust-Mantle Decoupling. *Tectonics*, 36(12):3135–3154, Dec. 2017. doi: 10.1002/2016tc004443.
- Markušić, S., Stanko, D., Penava, D., Ivančić, I., Bjelotomić Oršulić, O., Korbar, T., and Sarhosis, V. Destructive M6.2 Petrinja

- Earthquake (Croatia) in 2020—Preliminary Multidisciplinary Research. *Remote Sensing*, 13(6):1095, Mar. 2021. doi: 10.3390/rs13061095.
- MedNet Project Partner Institutions. Mediterranean Very Broadband Seismographic Network (MedNet), 1990. doi: 10.13127/s-d/fbbbtdtd6q. [Dataset].
- Minson, S. E. and Dreger, D. S. Stable inversions for complete moment tensors. *Geophysical Journal International*, 174(2): 585–592, Aug. 2008. doi: 10.1111/j.1365-246x.2008.03797.x.
- Mustać, M. and Tkalčić, H. Point source moment tensor inversion through a Bayesian hierarchical model. *Geophysical Journal International*, 204(1):311–323, Nov. 2016. doi: 10.1093/gji/ggv458.
- Mustać, M. and Tkalčić, H. On the Use of Data Noise as a Site-Specific Weight Parameter in a Hierarchical Bayesian Moment Tensor Inversion: The Case Study of The Geysers and Long Valley Caldera Earthquakes. *Bulletin of the Seismological Society of America*, May 2017. doi: 10.1785/0120160379.
- Mustać, M., Tkalčić, H., and Burky, A. L. The Variability and Interpretation of Earthquake Source Mechanisms in The Geysers Geothermal Field From a Bayesian Standpoint Based on the Choice of a Noise Model. *Journal of Geophysical Research: Solid Earth*, 123(1):513–532, Jan. 2018. doi: 10.1002/2017jb014897.
- Mustać, M., Hejrani, B., Tkalčić, H., Kim, S., Lee, S.-J., and Cho, C.-S. Large Isotropic Component in the Source Mechanism of the 2013 Democratic People's Republic of Korea Nuclear Test Revealed via a Hierarchical Bayesian Inversion. *Bulletin of the Seismological Society of America*, 110(1):166–177, Jan. 2020. doi: 10.1785/0120190062.
- Orecchio, B., Presti, D., Scolaro, S., and Totaro, C. Seismic deformation in the Adriatic Sea region. *Journal of Geodynamics*, 155: 101956, Mar. 2023. doi: 10.1016/j.jog.2022.101956.
- Palano, M. On the present-day crustal stress, strain-rate fields and mantle anisotropy pattern of Italy. *Geophysical Journal International*, 200(2):969–985, Feb. 2015. doi: 10.1093/gji/ggu451.
- Phạm, T. S. and Tkalčić, H. Toward Improving Point-Source Moment-Tensor Inference by Incorporating 1D Earth Model's Uncertainty: Implications for the Long Valley Caldera Earthquakes. *Journal of Geophysical Research: Solid Earth*, 126(11), Nov. 2021. doi: 10.1029/2021jb022477.
- Phạm, T. S., Tkalčić, H., Hu, J., and Kim, S. Towards a new standard for seismic moment tensor inversion containing 3-D earth structure uncertainty. *Geophysical Journal International*, 238(3): 1840–1853, July 2024. doi: 10.1093/gji/ggae256.
- Piccardi, L., Sani, F., Moratti, G., Cunningham, D., and Vittori, E. Present-day geodynamics of the circum-Adriatic region: An overview. *Journal of Geodynamics*, 51(2–3):81–89, Mar. 2011. doi: 10.1016/j.jog.2010.09.002.
- Pondrelli, S. European-Mediterranean Regional Centroid-Moment Tensors Catalog (RCMT), 2002. doi: 10.13127/rcmt/euromed. [Dataset]. Last accessed on 10 October 2024.
- Rovida, A., Locati, M., Camassi, R., Lolli, B., and Gasperini, P. The Italian earthquake catalogue CPTI15. *Bulletin of Earthquake Engineering*, 18(7):2953–2984, Mar. 2020. doi: 10.1007/s10518-020-00818-y.
- Rovida, A., Locati, M., Camassi, R., Lolli, B., Gasperini, P., and Antonucci, A. Catalogo Parametrico dei Terremoti Italiani (CPTI15), versione 4.0, 2022. https://emidius.mi.ingv.it/CPTI15-DBMI15/.
- Rösler, B. and Stein, S. Consistency of Non-Double-Couple Components of Seismic Moment Tensors with Earthquake Magnitude and Mechanism. *Seismological Research Letters*, 93(3): 1510–1523, Feb. 2022. doi: 10.1785/0220210188.
- Saoulis, A. A., Piras, D., Spurio Mancini, A., Joachimi, B., and Fer-

- reira, A. M. G. Full-waveform earthquake source inversion using simulation-based inference. *Geophysical Journal International*, 241(3):1741–1762, Mar. 2025. doi: 10.1093/gji/ggaf112.
- Schmid, S. M., Fügenschuh, B., Kounov, A., Maţenco, L., Nievergelt, P., Oberhänsli, R., Pleuger, J., Schefer, S., Schuster, R., Tomljenović, B., Ustaszewski, K., and van Hinsbergen, D. J. Tectonic units of the Alpine collision zone between Eastern Alps and western Turkey. *Gondwana Research*, 78:308–374, Feb. 2020. doi: 10.1016/j.gr.2019.07.005.
- Scognamiglio, L., Tinti, E., and Michelini, A. Real-Time Determination of Seismic Moment Tensor for the Italian Region. *Bulletin of the Seismological Society of America*, 99(4):2223–2242, July 2009. doi: 10.1785/0120080104.
- Sector for Seismology, Institute of Hydrometeorology and Seismology of Montenegro. Montenegrin Seismic Network, 1982. doi: 10.7914/SN/ME. [Dataset].
- Shang, X. and Tkalčić, H. Point-Source Inversion of Small and Moderate Earthquakes From P-wave Polarities and P/S Amplitude Ratios Within a Hierarchical Bayesian Framework: Implications for the Geysers Earthquakes. *Journal of Geophysical Research: Solid Earth*, 125(2), Jan. 2020. doi: 10.1029/2019jb018492.
- Sipkin, S. A. Interpretation of non-double-couple earthquake mechanisms derived from moment tensor inversion. *Journal* of Geophysical Research: Solid Earth, 91(B1):531–547, Jan. 1986. doi: 10.1029/jb091ib01p00531.
- Slovenian Environment Agency. Seismic Network of the Republic of Slovenia, 1990. doi: 10.7914/SN/SL. [Dataset].
- Stipčević, J., Herak, M., Molinari, I., Dasović, I., Tkalčić, H., and Gosar, A. Crustal Thickness Beneath the Dinarides and Surrounding Areas From Receiver Functions. *Tectonics*, 39(3), Mar. 2020. doi: 10.1029/2019tc005872.
- Tape, W. and Tape, C. A geometric setting for moment tensors: A geometric setting for moment tensors. *Geophysical Journal International*, 190(1):476–498, May 2012. doi: 10.1111/j.1365-246x.2012.05491.x.
- Tkalcic, H., Dreger, D. S., Foulger, G. R., and Julian, B. R. The Puzzle of the 1996 Bardarbunga, Iceland, Earthquake: No Volumetric Component in the Source Mechanism. *Bulletin of the Seismological Society of America*, 99(5):3077–3085, Sept. 2009. doi: 10.1785/0120080361.
- Tomljenović, B., Csontos, L., Márton, E., and Márton, P. Tectonic evolution of the northwestern Internal Dinarides as constrained by structures and rotation of Medvednica Mountains, North Croatia. *Geological Society, London, Special Publications*, 298(1):145–167, Jan. 2008. doi: 10.1144/sp298.8.
- Torbar, J. Izvješće o zagrebačkom potresu 9. studenoga 1880. Djela Jugoslavenske akademije znanosti i umjetnosti, knjiga I, 1882. JAZU, Zagreb (in Croatian).
- University of Bari "Aldo Moro". OTRIONS, 2013. doi: 10.7914/S-N/OT. [Dataset].
- University of Zagreb. Croatian Seismograph Network, 2001. doi: 10.7914/SN/CR. [Dataset].
- van Hinsbergen, D. J., Torsvik, T. H., Schmid, S. M., Maţenco, L. C., Maffione, M., Vissers, R. L., Gürer, D., and Spakman, W. Orogenic architecture of the Mediterranean region and kinematic reconstruction of its tectonic evolution since the Triassic. *Gondwana Research*, 81:79–229, May 2020. doi: 10.1016/j.gr.2019.07.009.
- Vasyura-Bathke, H., Dettmer, J., Dutta, R., Mai, P. M., and Jónsson, S. Accounting for theory errors with empirical Bayesian noise models in nonlinear centroid moment tensor estimation. *Geophysical Journal International*, 225(2):1412–1431, Jan. 2021. doi: 10.1093/gji/ggab034.
- Vavryčuk, V. Moment tensor decompositions revisited. Journal of

- *Seismology*, **19(1):231–252**, Oct. **2014**. doi: 10.1007/s10950-014-9463-y.
- Z.A.M.G. Zentralanstalt für Meterologie und Geodynamik. Austrian Seismic Network, 1987. doi: 10.7914/SN/OE. [Dataset].
- Zhao, L.-S. and Helmberger, D. Source Estimation from Broadband Regional Seismograms. *Bulletin of the Seismological Society of America*, 84(1):91–104, 1994. doi: 10.1785/bssa0840010091.
- Zhu, L. and Helmberger, D. V. Advancement in source estimation techniques using broadband regional seismograms. *Bulletin of the Seismological Society of America*, 86(5):1634–1641, Oct. 1996. doi: 10.1785/bssa0860051634.
- Šavor Novak, M., Uroš, M., Atalić, J., Herak, M., Demšić, M., Baniček, M., Lazarević, D., Bijelić, N., Crnogorac, M., and Todorić, M. Zagreb earthquake of 22 March 2020 preliminary report on seismologic aspects and damage to buildings. *Journal of the Croatian Association of Civil Engineers*, 72(10):869–893, Oct. 2020. doi: 10.14256/jce.2966.2020.

The article Bayesian Reassessment of Seismic Moment Tensors and Their Uncertainties in the Adriatic Sea Region © 2025 by Jinyin Hu is licensed under CC BY 4.0.